Normal fault growth in continental rifting: insights from changes in displacement and length fault populations due to increasing extension in the central Kenya Rift

Ahmad K. Shmela [a,]*, Douglas A. Paton [b], Richard E Collier [c], Rebecca E. Bell [d]

[a, c] University of Leeds, School of Earth and Environment
[b]TectonKnow Ltd., Settle, North Yorkshire
[d] Imperial College London, Department of Earth Science & Engineering

---

Keywords: Scaling properties, Strain accommodation, Fault growth, Rift evolution

Highlights

- Examination of upper crust brittle deformation during continental rifting from DEM data.
- Examination of fractal dimension of power law fit of fault populations with increasing strain.
- Determination of fault growth models from fault population scaling properties.

Abstract

This study examines the scaling relationship between fault length and displacement for the purpose of gaining a better understanding of the evolution of normal faults within the central Kenya Rift. 620 normal faults were manually mapped from a digital elevation model (DEM), with 30 m^2 resolution and an estimated maximum displacement of ~40 – ~6030 m and fault lengths of 1270 - 60600 m. To assess the contribution of fault populations to the strain accommodation from south to north**,** the study area has been divided into three zones of fault populations based upon their average fault orientations; zone 1 in the north is dominated by NNE striking faults, zone 2 in the centre of the rift is characterised by NNW to NNE fault trends, whereas zone 3 in the south is characterised by NNW striking fault systems. Extensional strain was estimated by summing fault heaves across six transects along the rift, which showed a progressive increase of strain from south to north. The fault length and displacement data in the three zones fit to a power law distribution. The cumulative distributions of fault length populations showed similar fractal dimension (D) in the three zones. The cumulative displacement distributions for the three zones showed a decrease in the Power-law fractal dimension with increasing strain, which implies that the strain is increasingly localised onto larger faults as the fault system becomes more evolved from south to north. Increasing displacement with increasing strain while the fault length remains almost constant may indicate that the fault system could be evolving in accordance with a constant length fault growth model, where faults lengthen quickly and then accrue displacement. Results of this study suggest that the process of progressively increasing fault system maturity

and strain localization onto large faults can be observed even over a relatively small area (240 x 150 km) within the rift system. It is also suggested that patterns of fault growth can be deduced from the fractal dimension of cumulative distribution of fault size populations.

1 Introduction

Observations of fault size, specifically displacement versus length distributions can be used to help understand rift development (e.g.Gupta and Scholz, 2000). Moreover, in order to understand the surface deformation of tectonically active regions, it is critical to understand the evolution of normal faulting associated with rifting and extensional processes.

Quantitative analyses of fault population parameters, such as trace-length, and displacement as well as displacement distributions have been studied in recent decades in many studies (e.g.Cowie and Scholz, 1992a, Dawers et al., 1993, Schultz and Fossen, 2002, Walsh et al., 2002b, Soliva and Schultz, 2008, Torabi and Berg, 2011, Torabi et al., 2019) in order to understand the growth history of fault populations. Such analyses have also been used to suggest a number of fault growth models including fault growth by radial propagation (Walsh and Watterson, 1988), a coherent fault model of segment linkage of fault arrays by Cartwright et al. (1995) and an alternative fault growth model suggested by e.g. Walsh et al. (2002a) and Rotevatn et al. (2019), where fault lengths are near constant from an early stage and growth is largely achieved by an increase in fault displacement.

Cumulative frequency distribution functions (CDF) are the most common way to describe attributes of fault populations (e.g. length, displacement) and have been used in many studies (e.g. Walsh et al., 1991, Jackson and Sanderson, 1992, Cladouhos and Marrett, 1996, Bonnet et al., 2001). Most populations of fault lengths and displacements have been found to plot along a more or less straight line in log-log space (e.g. fault length vs. cumulative number) which implies a power-law distribution (e.g. Watterson et al., 1996, Ackermann and Schlische, 1997, Poulimenos, 2000, Gillespie et al., 2001, Peacock, 2002, Bailey et al., 2005, Soliva and Schultz, 2008, Torabi et al., 2019). This power-law distribution is described mathematically as:

$$N=aS^{-D}$$

where S is fault offset (i.e. length, displacement, throw or heave), N is the cumulative number of fault offset, and a is a constant. D is an exponent, and it describes the fractal dimension of slope of the straight segment (Walsh et al., 1991, Yielding et al., 1996)

It has been demonstrated in several studies that differences in the value of the exponent D (the fractal dimension) are attributed to variations in the amount of strain accommodated by fault systems, and it may also change for different stages of fault evolution (i.e. fault nucleation, propagation and amalgamation) (e.g. (e.g. Cowie et al., 1995, Cowie, 1998a, Ackermann et al., 2001, Bailey et al., 2005). It has also been found that the fractal dimension is inversely related to the strain, where the former decreases systematically as the latter increases and vice versa (e.g. Cartwright et al., 1995, Poulimenos, 2000, Moriya et al., 2005). Therefore, analysis of the fractal dimension of power law distributions can be used to characterize the spatial distribution of faults (Cowie, 1998a, Sornette et al., 1993). It was also found that high fractal dimensions reflect a greater proportion of small faults relative to larger faults than lower fractal dimensions (Marrett and Allmendinger, 1991, Yielding et al., 1996)

The aims of this paper are to quantitatively investigate fault scaling relations (fault length and displacement) of three different fault populations for the purpose of providing insights into the evolution of normal fault systems in the central Kenya Rift. To achieve this aim, a Digital Elevation Model (DEM) with 30 m horizontal resolution is used to produce a detailed fault geometry dataset for surface faults of the central Kenya Rift. 620 faults have been manually mapped from this DEM over an area measuring 240 x 150 km. In this study, we measured the throw and length of surface faults derived from ASTER DEM data. Second, we estimated the part of fault throws obscured due to burial by volcanics and sediments in the hanging wall. Fault throw was then used to calculate the maximum displacement using an average fault dip for the central Kenya rift. The effect of data resolution on the fault trace length was also corrected by adding an estimated tip length. Next, three domains of differing fault populations have been identified, which offer an opportunity to investigate fault scaling relations of the fault populations along the central Kenya Rift during progressive deformation. Finally, we discuss the results addressing implications for the evolution of the rift and the growth of normal faults in the study area.

2 Tectonic and geological background

The spatial extent of this study covers a portion of the central Kenya Rift located between Lat 1.05º N to -1º S and Long 35.5º to 36.7º E that covers an area of 240 x 150 km (Figure 1). The central Kenya Rift is thought to represent a phase of relatively early continental rifting (Baker and Wohlenberg, 1971) where most deformation is accommodated on small boundary faults with an absence of internal faults (e.g. Corti, 2009, Agostini et al., 2011b). The northern part of the central Kenya Rift comprises two parallel Rift valleys (Figure 2). The eastern rift is known as the Kenya Rift and the western one is called the Kerio Rift, separated by the Kamasia horst, and these structures are oriented N10ºE (Figure 2). Both Rift basins are west-dipping half-grabens, with major border faults on the western rift shoulders, the Kerio Rift terminating west of Lake Bogoria, while the Kenya Rift continues farther to the south and bends sharply at the Gregory Rift (Figure 2). This bend has been interpreted as the intersection with a large NW trending basement structure known as the Aswa lineament (Smith and Mosley, 1993, Chorowicz, 2005, Omenda, 2010).

The central segment of the Kenya rift system is known as the Gregory Rift (Figure 2) and is a complex graben that trends N-S. It is 60 -70 km in width and is bounded by en echelon arrangements of major normal faults forming the Nguruman, Mau, and Elgeyo escarpments on the western boundary and the Aberdare escarpment on the eastern boundary (Jones and Lippard, 1979, Baker et al., 1988) (Figure 2). Fault escarpments are well defined and reach up to 2000 m in height (Baker and Wohlenberg, 1971). The central Kenya rift encompasses a number of half graben basins that have varying orientations ranging from NNE-SSW to NNW-SSE (Smith and Mosley, 1993). The major faults in the central Kenya Rift are antithetic and dominantly dip eastwards (Baker and Wohlenberg, 1971, Baker et al., 1972). Overall, the tectonostratigraphic evolution of these Rift sectors shows a successive migration of normal faulting from the boundary faults inwards toward the Rift valley , where the structural development has been characterized by a concentration of faulting associated with volcanism since late Pliocene era (Baker and Wohlenberg, 1971).

Volcanism and rifting started in the Kenya Rift around the early Miocene in the north, in the Lake Turkana area and migrated southwards. Rifting was active from around the middle to late Miocene in the central segment (Baker et al., 1972, Smith and Mosley, 1993). The Kerio basin in the centre and the Baringo basin in the north of the central Kenya Rift witnessed a long period of extensive basaltic lava extrusion during the initial phase of rifting (Paleogene to lower Miocene) (Ebinger, 1989). Therefore, infill in the central Kenya Rift is predominantly volcanogenic (Smith, 1994). Furthermore, a geological map of Kenya (Ministry of energy of Kenya 1987, Figure 1) shows that the study area is covered by Quaternary and Tertiary volcanic sediments. The thickness of sediments and volcanic deposits in this region is ~4.5-5km (Hautot et al., 2000) as determined from magnetotelluric (MT) data, which is a geophysical method used to model the Earth's subsurface from measurements of natural geomagnetic and geoelectric field variation at the Earth's surface.

It has been proposed that faults in the East African Rift System (EARS) are not randomly distributed but tend to follow the trend of pre-existing weakness zones within the lithosphere i.e. Proterozoic mobile belts, and avoid the Archaean stable cratonic areas (McConnell, 1972, Daly et al., 1989, Petit and Ebinger, 2000, Ziegler and Cloetingh, 2004). The central Kenya Rift segments formed along old zones of weakness at the contact between two contrasting types of lithosphere; the Archean Tanzanian craton and the Proterozoic Mozambique belt (e.g. Smith and Mosley, 1993, Mariita and Keller, 2007). Therefore, the extensional deformation may be localized along mobile belts and suture zones as they tend to be weaker than the surrounding areas (Petit and Ebinger, 2000).

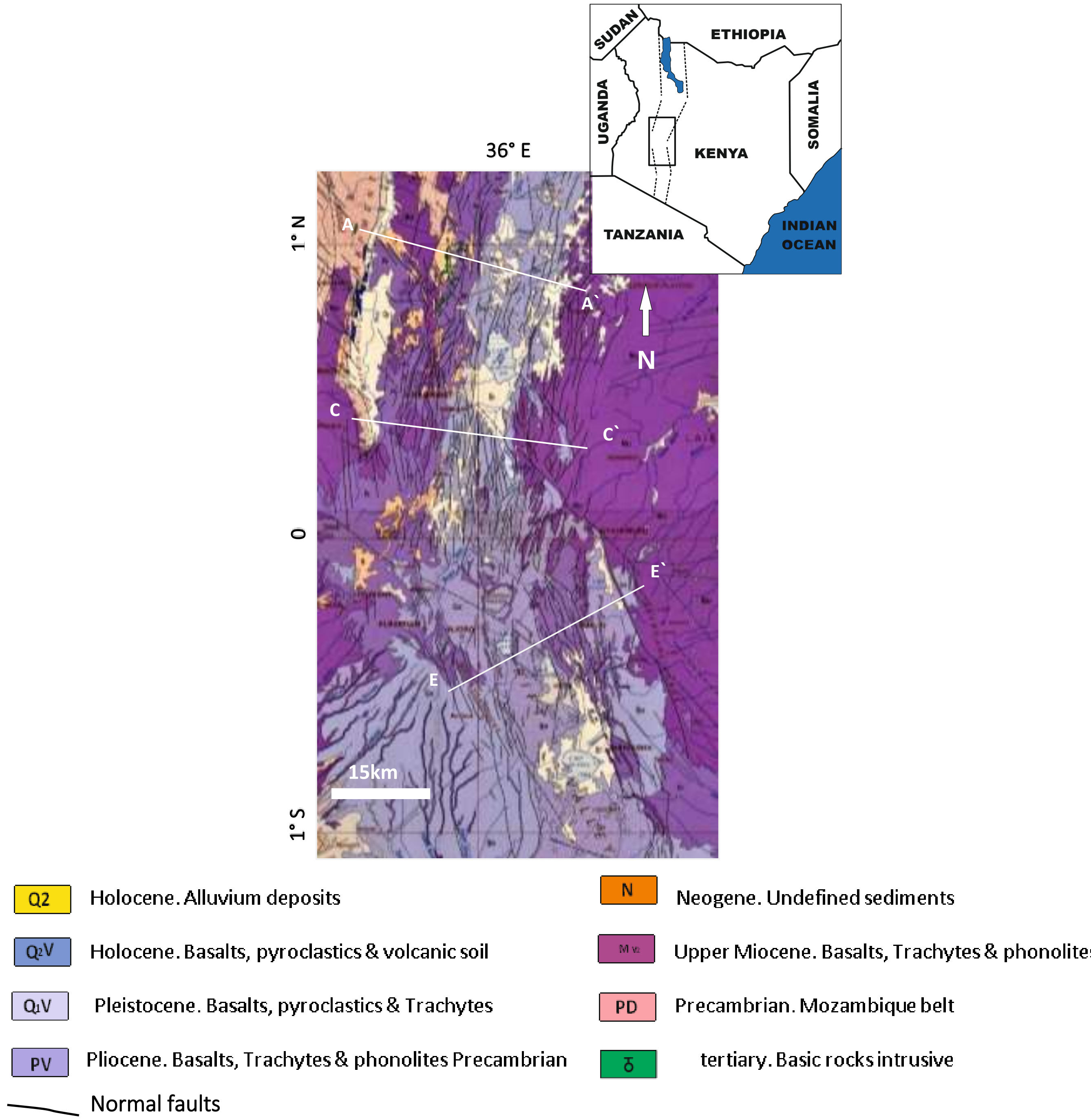

Figure 1. a geological map of the study area, from geological map of Kenya (Ministry of Energy of Kenya 1987). The small inset image displays the location of the study area, the central Kenya rift. The white lines are locations of the topographic profile shown in figure 8.

3 Methodology

3.1 Data and interpretation of fault traces

In this study, 620 discrete faults were identified, from which fault measurements were made such as fault trace length, maximum apparent throw, orientation, and throw\length ratio. Maximum apparent displacement was derived from each maximum fault throw value using an average fault dip of 65°. There are several reasons for using an average fault dip in this regional study: firstly, fault dips cannot be directly measured from ASTER DEM data. Secondly, lack of fault dip data in previous studies for the study area and thirdly, the large number of faults involved in this study that required a generalized assumption. This fault dip value of 65° is the average of a fault dip range of 55° to 75° for the central Kenya Rift as reported in Zielke and Strecker (2009).

Digital elevation models (DEM) are the main data used to investigate the upper crust brittle deformation in the study area. The DEM data were obtained from the USGS (https://lpdaac.usgs.gov/) through Advanced Space-borne Thermal Emission and Reflection Radiometer (ASTER) data with ground resolution of 30 m x 30 m and vertical resolution of 20 m to provide information on the morphology of surface faults. Google Earth optical spectrum imagery with a resolution of about 15 m was used along with the ASTER DEM to assist in viewing the topography and determine the dip direction of the mapped faults. The data resolution refers to the minimum distance by which data can be recorded from the scanned scene. The main effect of resolution is a truncation, which means fault trace lengths below 30 m (found in fault tips) and fault heights (throws) below 20 m cut-offs are not resolvable, which lead to underestimation of these parameters. However, the effect of truncation is more significant on small size fault populations (Walsh et al., 1996, Watterson et al., 1996, Yielding et al., 1996)

The DEM data were converted into a shaded relief surface (Figure 2). Fault traces were identified on the DEM surface by using several techniques available in Petrel software, including edge detection, which is particularly useful in identifying where subtle changes in the surface topography occur, thereby enhancing confidence in mapping fault escarpments. Vertical exaggeration of x5 was also used to facilitate tracing fault scarps. Given the resolution of the DEM used, some topographic features (i.e. <20 m height) that do not show clear topographic scarps were not considered to be faults. Nevertheless, hundreds of fault scarps were readily distinguishable on the DEM surface across the study area. Fault scarps were interpreted and recorded based on their length, and when fault segments were linked, the entire length of the fault segment array was mapped as a single larger fault.

In this study, the height of fault scarp measured from the DEM has been used as a proxy for fault throw. However, accumulation of sediment, volcanic and erosional deposits reduce the apparent height of the fault scarp. Moreover, fault blocks are normally eroded, and in DEM surfaces, it is not possible to determine how much erosion of the block has occurred. All these uncertainties may introduce systematic error into throw measurements and strain estimations. For each fault, footwall cut-offs were manually digitized by tracing the crest of each topographic scarp along strike (blue dots on blue lines in Figure 3A –C), whilst apparent hanging wall cut-offs were picked by tracing the lower-most position of the fault along its trace (pink dots on pink lines in Figure 3A – C). Therefore, the measured throw was the maximum value of the apparent fault height/ throw between the corresponding points picked in the footwall cut-off and the hanging wall cut-off along each fault trace measured in two dimensions (2D). Fault length defined in this study is the horizontal exposed fault trace length along strike.

The chronology of fault formation in the central Kenya rift is that major faults were first formed between 16 and 8 Ma (Smith, 1994), and the volcano-sedimentary infill in the rift is between 4.5-5km thick (Hautot et al. (2000). Consequently, fault throws, and lengths measured at this stage are just the apparent or exposed values of fault throw, and length due to possibility of hanging walls being partially filled with sediment, volcanic and erosional deposits, and subsequent burial of fault tips.

175

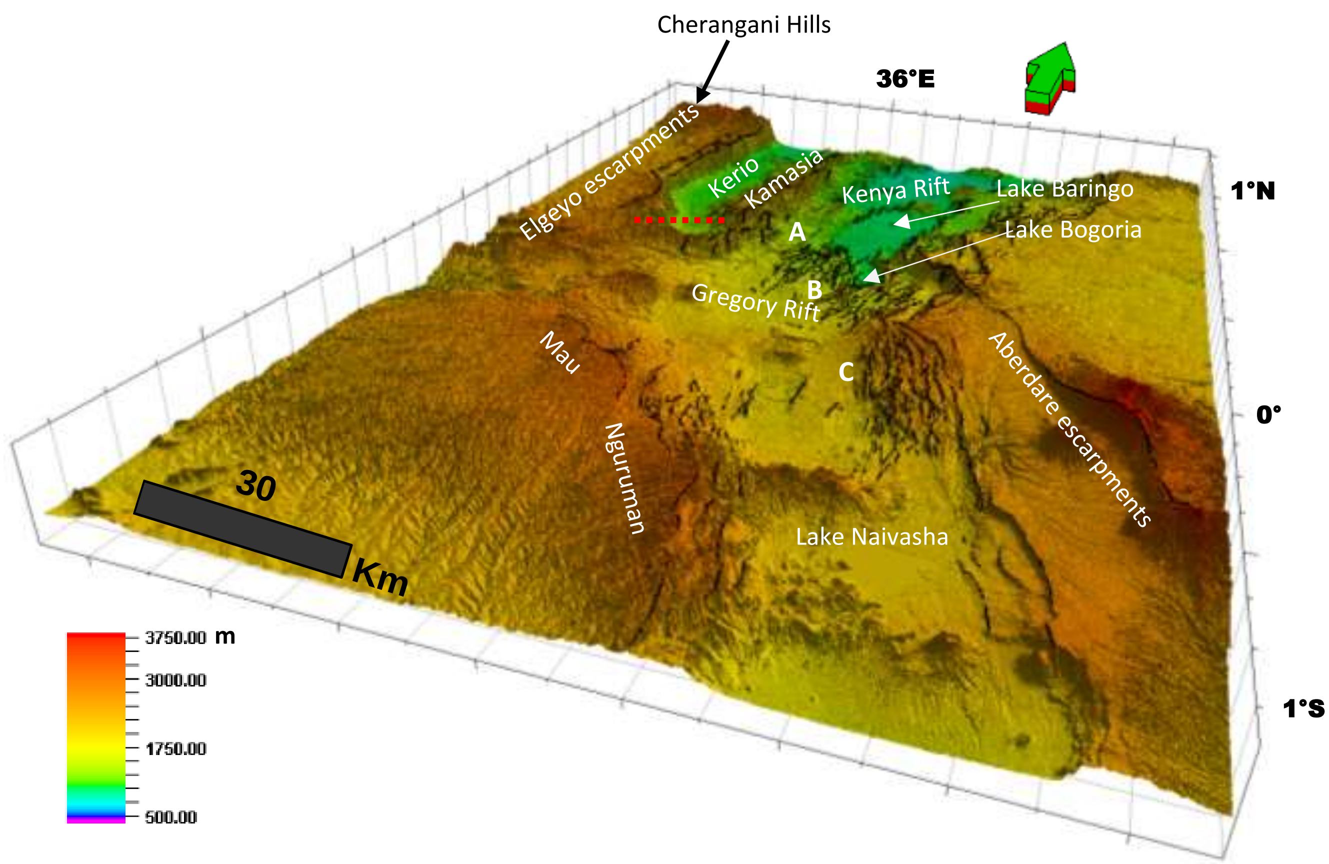

Figure 2. A shaded relief surface image generated from ASTER DEM. The small inset image displays location of study area within the East Africa Rift System; dashed red line is a location of seismic line shown in (Figure 4); A, B and C are locations of close-up images (Figure 3)

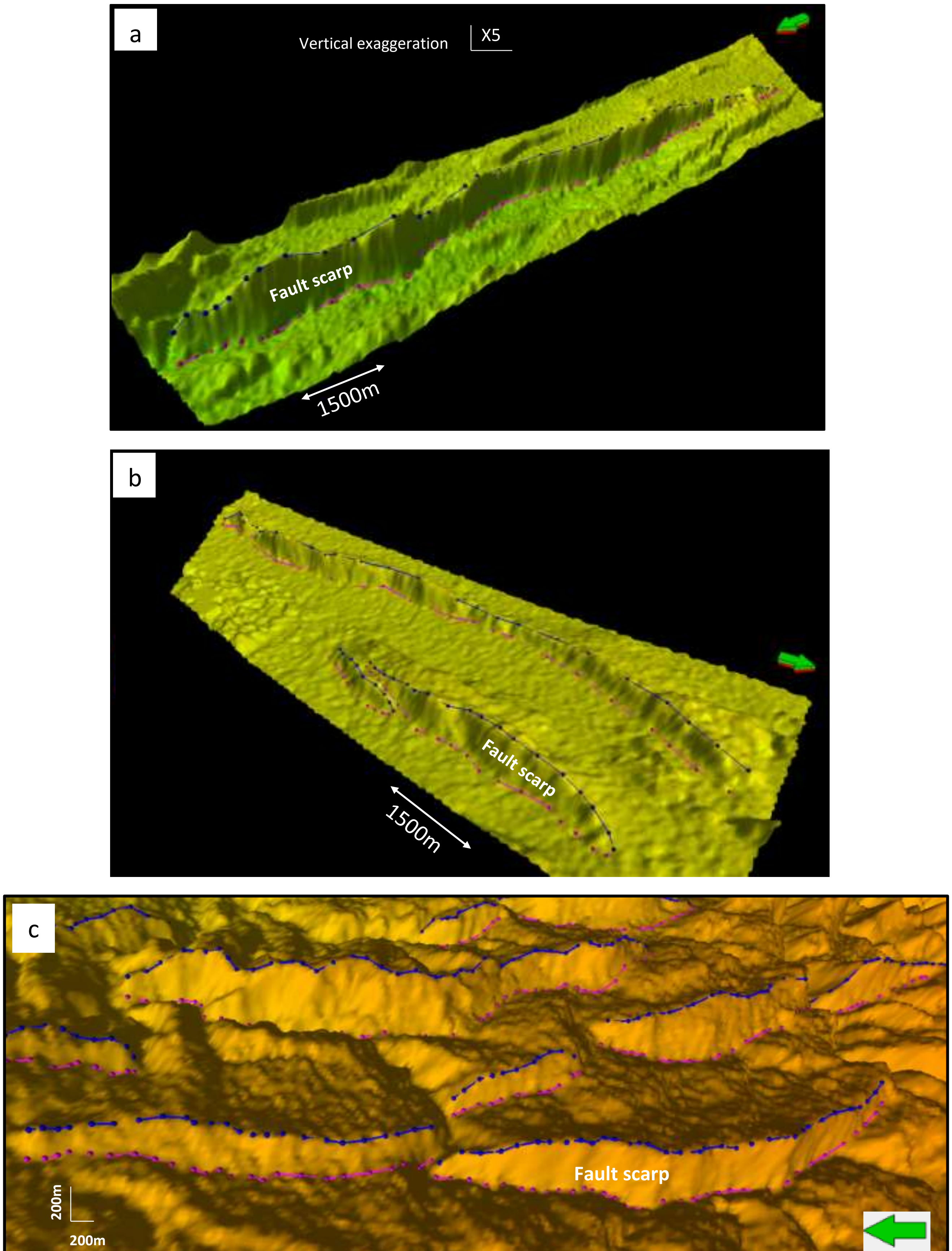
a
Vertical exaggeration
X5
Fault scarp
1500m
b
Fault scarp
1500m
c
Fault scarp
200m
200m

Figure 3. Examples to show how the faults were picked using the DEM surface. The footwall cut-off is picked (shown as blue circles on blue polyline) followed by picking the corresponding apparent hanging wall cut-off (pink circles on pink polyline), resulting in the same number of picks top and bottom, which were used to calculate throw. a) Fault scarp structure shows the final picks for the footwall and hanging wall cut-offs. b) Fault structure on the left-hand side of the image is an example of fault picking along two faults separated by a relay ramp. c) Picks along several en echelon fault scarps in the central part of the study area. (See Figure 2 for image locations).

3.2 Under sampling of faults lengths due to truncation bias.

Data resolution and burial of fault tips may mask the true positions of fault tips at the surface and therefore cause fault lengths to be underestimated. Truncation bias refers to effects caused by systematic under-representation of smaller faults in a sample due to limitations in data resolution, below which the fault length and throw cannot be detected (Pickering et al., 1995, Watterson et al., 1996, Zhang and Einstein, 2000, Bonnet et al., 2001). This truncation bias needs to be corrected for, to provide a more reliable estimate of the fault trace length. However the effects of truncation are relatively more significant on small scale fault populations (Walsh et al., 1996, Watterson et al., 1996, Yielding et al., 1996). Censoring bias refers to partial sampling of large faults that extend beyond the sample area and therefore are incompletely characterized (Pickering et al., 1995, Zhang and Einstein, 2000, Bonnet et al., 2001). Censoring is thought to not be of great significance unless the sample area is small relative to the full lengths of the majority of fault traces (Heffer and Bevan, 1990).

It has been shown in some studies such as Pickering et al. (1997) and Soliva and Schultz (2008) that the truncation bias can be estimated by dividing the lowest throw value that can be resolved by the average value of throw/length ratio in a given region. The average throw/length ratio calculated for this study area was 0.04, which is similar to that estimated by Le Gall et al. (2008), in southern Kenya close to the Tanzania border. Given the vertical resolution of 20m ASTER DEM (https://lpdaac.usgs.gov/), we estimate that a truncation bias occurs for fault lengths less than 500 m. To account for the truncation bias, we added a 500 m to the end of each fault to enable us to estimate the true distribution of fault lengths. By adding the 500 m to fault tips of the 620 mapped faults, the length populations range from 1270 m to 60600 m, with an average length of 6150 m.

3.3 Under sampling of fault throws and derivation of displacements

In this study we quantified throw as the height of the fault scarp measured from the DEM. The extent of total fault throws into the subsurface is hard to be constrained due to the scarcity of seismic data over this region of the EARS. However, a seismic line (Figure 4b) shown in Morley and Ngenoh (1999c) was used in an attempt to account for the missing throw. This seismic line was shot by the National Oil Corporation of Kenya (NOCK) in 1990 over at the southern end of the Kerio Rift between the Elgeyo escarpment and the Kamasia horst (see Figure 2 for location). According to the interpretation by Pope (1992) and Ngenoh (1993), this seismic line shows a large boundary fault, namely the Elgayo Fault in the subsurface, which marks the western boundary of the Rift (Figure 4b). The DEM image resolves the continuation of the Elgayo escarpment at the surface (Figure 4a).

From the seismic line (Figure 4 b) we interpret the Elgayo Fault hanging wall cut-off to be at a depth of ~2 sec (TWT) (Figure 4c). Given that the average seismic velocity for the rift infill between Lake Baringo and Lake Naivasha is about 4000 m/s as determined by Henry et al. (1990b), the subsurface fault throw is therefore about 4 km. This value is in general agreement with the thickness of volcanic-sedimentary infill of ~4.5 km estimated in Hautot et al. (2000) using Magnetotellurics (MT), and an estimate of 4km in Henry et al. (1990b) that derived the thickness of the sediment/volcanics layer from two seismic refraction lines in the central Kenya Rift. Consequently, the buried throw is about 2.5 times the apparent throw of ~1560 m estimated from the surface scarp of the Elgeyo escarpment. Since there have been no detailed regional studies that recorded the volcano-sedimentary infill in different parts of the central Kenya rift, and also due to the lack of adequate subsurface data in this rift, the buried throw of different size faults across the rift cannot be established. Therefore, for simplicity, we assumed that all mapped faults extend under the surface by the same factor of 2.5 time as that calculated for the Egleyo escarpment. So, the correction consists of simply multiplying each surface apparent fault throw measurement by 2.5 and adding the apparent surface throw for each mapped fault. Consequently, the estimated maximum throw range is ~37 to ~5460 m with an average of ~450 m. Fault displacements were then derived from fault throws through a simple geometric calculation using a representative fault dip of 65°.

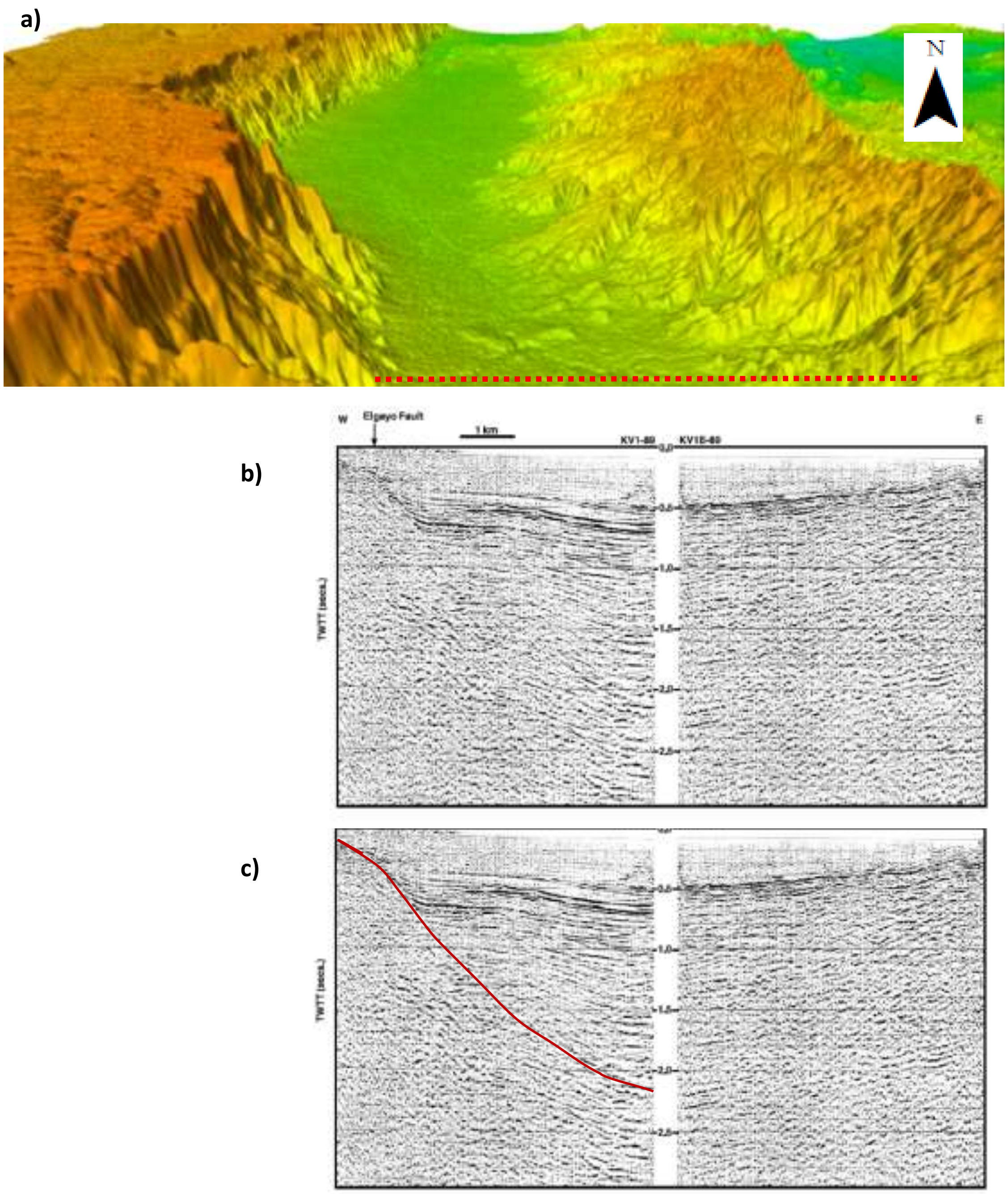

Figure 4. a) DEM surface showing the Elgayo Fault escarpment, dashed red line shows the location of seismic line, which is about 12 km in length (see Figure 1). b) seismic line in the Kerio Rift from Morley and Ngenoh (1999c). c) interpretation of the Elgayo Fault.

3.4 Fault analysis methods

As part of examining the 620 faults mapped from the DEM surface, the relationship between fault displacement and fault length is plotted and compared with a global data set of normal faults. It has been largely accepted that the relationship between displacement and fault length provides crucial information on the growth of faults through time (e.g. Walsh and Watterson, 1988, Cowie and Scholz, 1992b). The relationship between the maximum displacement (D) and the fault length (L) has been defined as follows (e.g. Walsh and Watterson, 1988, Dawers et al., 1993):

$$dmax = cL^n$$

where c is a constant relating to material properties, n is the exponent value, which ranges from 0.5 to 2.0 for tectonic fault systems. published values of n are; n = 0.5 (Fossen and Hesthammer, 1997), n =1.0 (Cowie and Scholz, 1992a, Dawers et al., 1993, Schlische et al., 1996, Davis et al., 2005, Stanton-Yonge et al., 2020), n =1.5 (Marrett and Allmendinger, 1991, Gillespie et al., 1992) and n =2.0 (Watterson, 1986, Walsh and Watterson, 1988), The n value of fault Displacement/Length data has implications for what fault model best describes the growth of faults.

In this paper, the trend of extensional strain from south to north of the study area was estimated by measuring total fault heave across faults along six transects along the rifts (Figure 3), in order to determine the contribution of different fault populations to the strain. The horizontal fault separation (heave) was estimated by measuring the horizontal distance between the hanging-wall and footwall cut-offs, measured perpendicular to the trace of the fault in map view (2D) for all faults that intersect the cross-sections. However, volcanic and sediment infill as well as eroded faults scarps prevent identifying the original positions of faults hanging wall and footwall cut-offs, which in turn would introduce some uncertainties on heave measurements. Moreover, the extensional strain may also be underestimated due to underrepresentation of small faults that fall below the resolution of observation.

Fault displacements and fault lengths were analysed through fault cumulative frequency plots. This can be done through ranking the displacement/length data in a descending order and then plotting fault displacement/length data against the cumulative frequency in a log-log scale. Different statistical functions (i.e. power law, lognormal and exponential laws) have been used to examine the best fit for the fault displacement/length data. These statistical functions deploy a transformed regression model, which is a type of least squares estimation method to fit statistical distributions that has been widely used in geological studies (Pickering et al., 1995, Poulimenos, 2000, Peacock, 2002, Bailey et al., 2005, Soliva et al., 2006, Soliva and Schultz, 2008).

4 Fault Population analysis and results

4.1 Relationship between fault length and displacement

Fault displacement and length data obtained in this study were compared with previously published displacement-length data (Figure 5) for normal faults from different sources compiled by Gillespie et al. (1992) and Bailey et al. (2005). The mapped faults lie well within the published global dataset.

Fault maximum displacement and length data from the three zones were plotted in different colors in a log-log space (Figure 6a). The data from the three zones combined showed a large scatter that spans about two orders of magnitude in both variables. A linear regression line passing through the data points is expressed as $y = 0.0691x^{+129.5}$ with coefficient of determination $R^2 = 0.479$ and a power law fit, with a slope of $n = 1.09$ and $R^2 = 0.382$. The low coefficient of determination together with the large extent of scatter cannot justify the regression lines. The maximum displacement-length data for each individual zone also exhibited a low coefficient of determination for both linear and power law trendlines due to the high scatter. Such scatter is common to other fault population studies and has been attributed to: combining data sets from areas of different lithology and material properties (e.g. Cartwright et al., 1995, Peacock and Sanderson, 1991, Peacock, 2002, Cowie and Scholz, 1992a), fault growth and segment linkage (Cartwright et al., 1995, Schlische et al., 1996, Cartwright et al., 1996, Mansfield and Cartwright, 2001), sampling effects and inaccurate measurement (Gillespie et al., 1992). However, despite this high scatter, it can be observed from displacement-length data for each individual zone (Figure 6b, c, d), where several faults have a comparable length but varying displacement, that this will lead to increasing displacement-length ratios for larger faults, and create a general vertical trend of increasing displacement for those faults which have fixed length but accumulate throw.

302

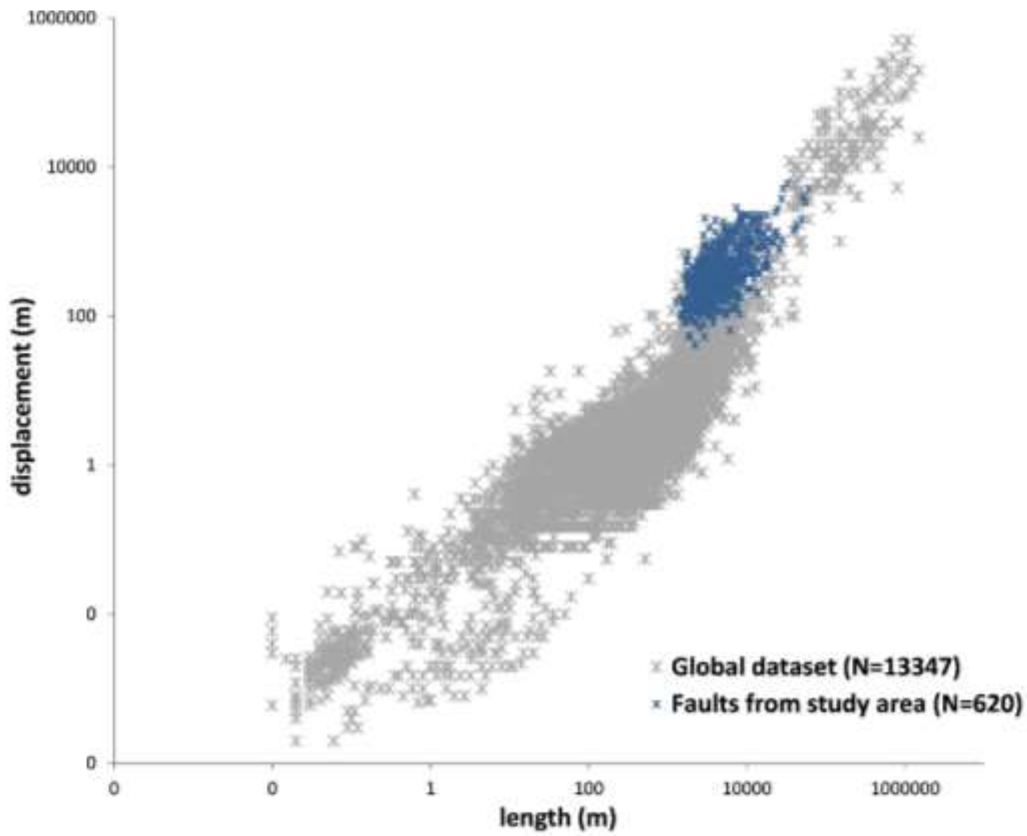

Figure 5. Log-log plot of fault displacement vs. length for faults from the study area along with previously published data from (Gillespie et al., 1992, Bailey et al., 2005).

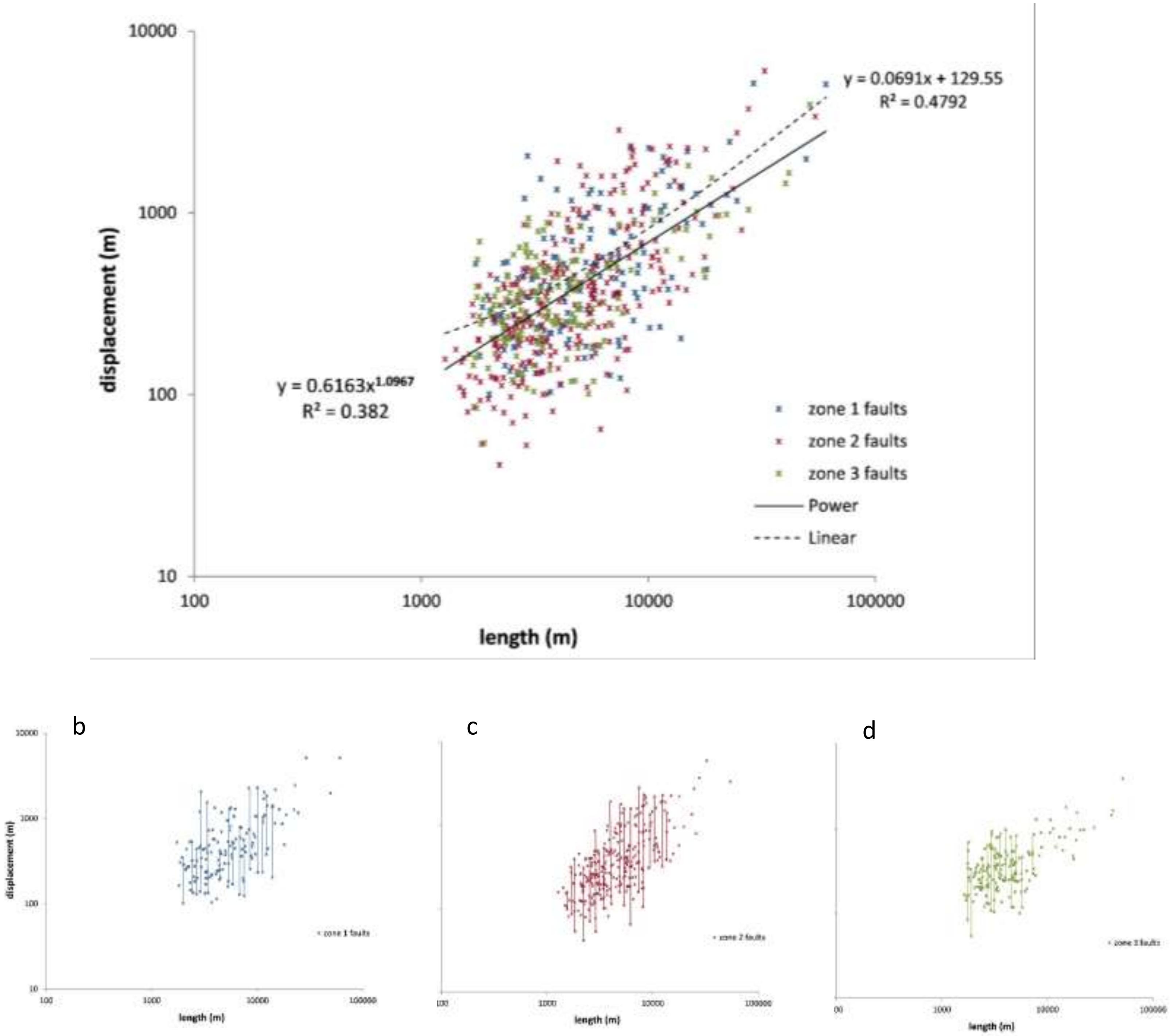

Figure 6. (a) Log-log plot for displacement vs length for all faults mapped in the study area showing a large scatter. (b, c & d) Displacement vs. length plots of individual fault zones, faults showing comparable length, but varying displacement are joined by lines to illustrate the observed vertical trend of increasing displacement population..

4.2 Relationships between strain and fault populations

There are different fault orientations throughout the study area (Figure 7). Therefore, to assess the contributions of different fault sets to the strain accommodation of the entire area, the region was divided into three subzones (zone 1, zone 2 & zone 3) based upon average fault orientations (Figure 7). Zone 1, in the north is dominated by N-NNE striking faults, zone 2 in the central section of the rift is characterised by a NNW to NNE fault strike, whereas zone 3 in the south is characterised by a N-NNW striking fault system (Figure 7). The number of resolved faults is 149, 295 and 177 for zone1, zone 2 and zone 3 respectively.

Normal faults typically form perpendicular to the stress direction. The average fault orientation for zone 3 (shown as a red line in the rose diagrams in Figure 7) is ~10°oblique from being perpendicular to the regional EW-trending extension orientation, and more oblique compared to zone 2 and zone 1. In theory, such obliquity would cause the displacement vector to deviate from true dip-slip and produce what is called an oblique-slip fault. However, the true displacement vector cannot be estimated from a DEM in such a regional study, because defining a fault as oblique requires both dip and strike components to be measurable and significant. Therefore, for the purpose of this study, we assumed the effect of ~10° obliquity between the average fault orientation and the EW-trending regional extension in zone 3 to be insignificant, and consequently error associated with calculating displacement from the apparent throw measurements to be also negligible.

4.3 Strain accommodation

Fault heaves are an expression of strain in extensional tectonic settings. Fault displacement (i.e. heave and throw) increases as strain accumulates (e.g. Poulimenos, 2000, Walsh et al., 2002a, Schlagenhauf et al., 2008). Therefore, in this study, we consider that total (cumulative) heave and associated heave percentage (Table 1) are illustrative of strain. The strain along the rift from south to north was then assessed using six cross-sections (Figure 7). The cross-sections were defined perpendicular to the trend of fault populations in each zone. We present two cross-sections for each zone, AA\` & BB\` in zone 1, CC\` & DD\` in zone 2 trend ESE-WNW and EE\`& FF\` in zone 3 trend ENE-WSW (Figure 7). Total fault heave that has been taken as representative of strain was then estimated by summing fault heaves across each cross-section. This analysis shows that average strain in each zone increases from ∼5560 m in zone 3 (south) to ∼7470 m in the central (zone 2), whereas zone 1 in the north exhibited the largest average extension of ∼ 9800 m (Table 1). The percentage of strain accommodated at each cross-section in relation to the overall strain of the study area was defined by dividing the amount of strain of each transect by the total amount of strain estimated for the entire study area (Table 1). Figure 9 shows a progressive increase of strain from zone 3 in the south to zone 1 in the north. Estimations of uncertainty in measurements of each total heave (**Error! Reference source not found.**) did not show a significant error contribution (Figure 9).

(Figure 8) shows topographic profiles of cross-sections AA`, CC` and EE respectively. These profiles show that the width of the rift valley widens from 19 km in the south (cross-section EE`) to 40 km in the north (cross-section AA`). Elevation of the rift valley also decreases from ~2000 m in the south (cross-section EE`) to ~1000 m in the north (cross-section AA`), where rift valleys of the Kero Rift and the Kenya Rift appear to be in the lowest part of the study area. This systematic decrease in rift floor elevation is interpreted to reflect increased lithospheric thinning and subsidence, as indicated by Cowie et al. (2005). The geological formations shown in the cross-sections depict extensive volcanic deposits along the rift as reported by Ebinger (1989).

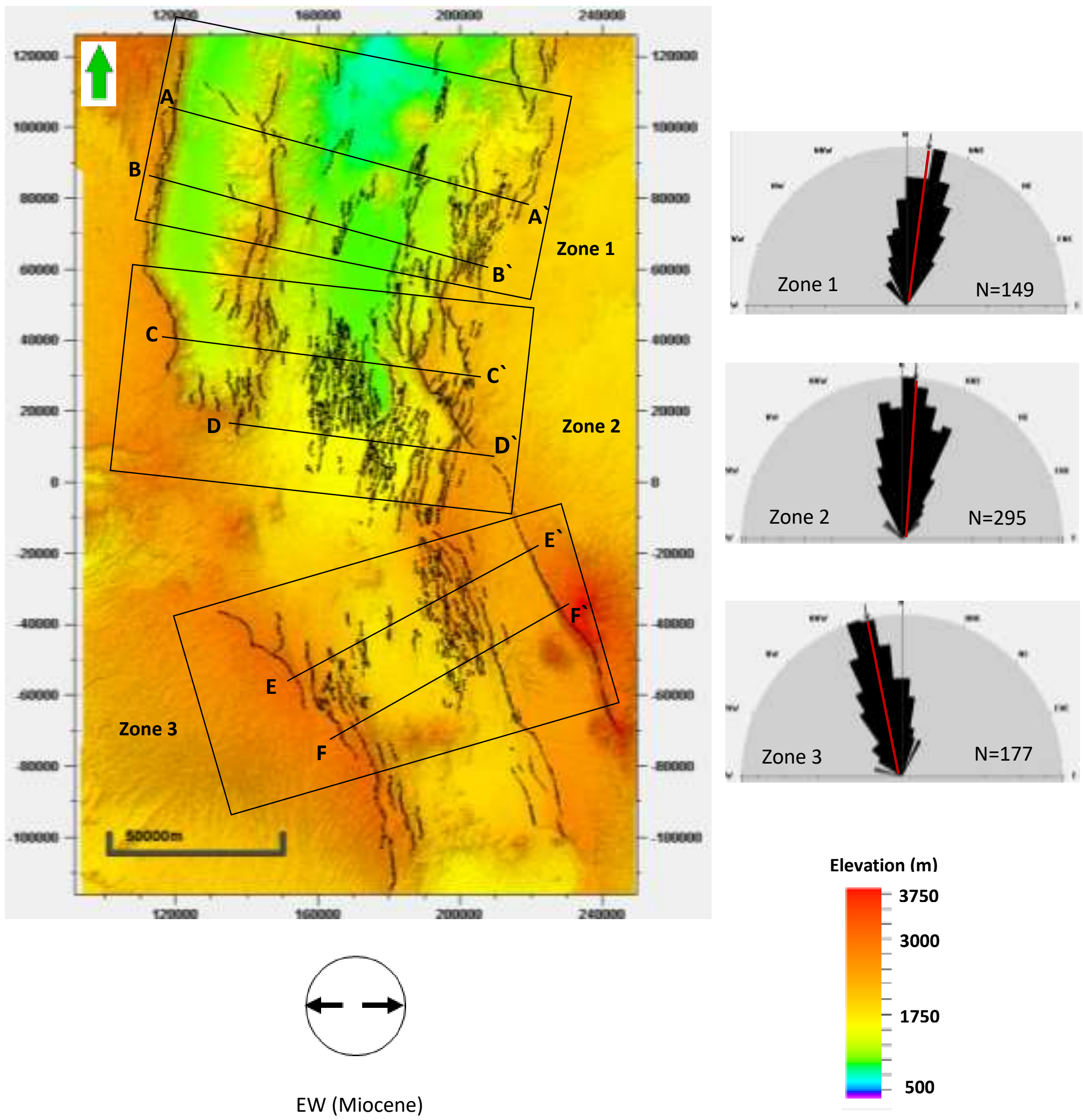

Figure 7 . Rectangles represent the three structural zones defined within the study area, and location of cross-sections (see Figure 2 for location of the 3D surface). The two opposite arrows indicate extension direction, and the red line within the rose diagrams shows the average orientation of fault population.

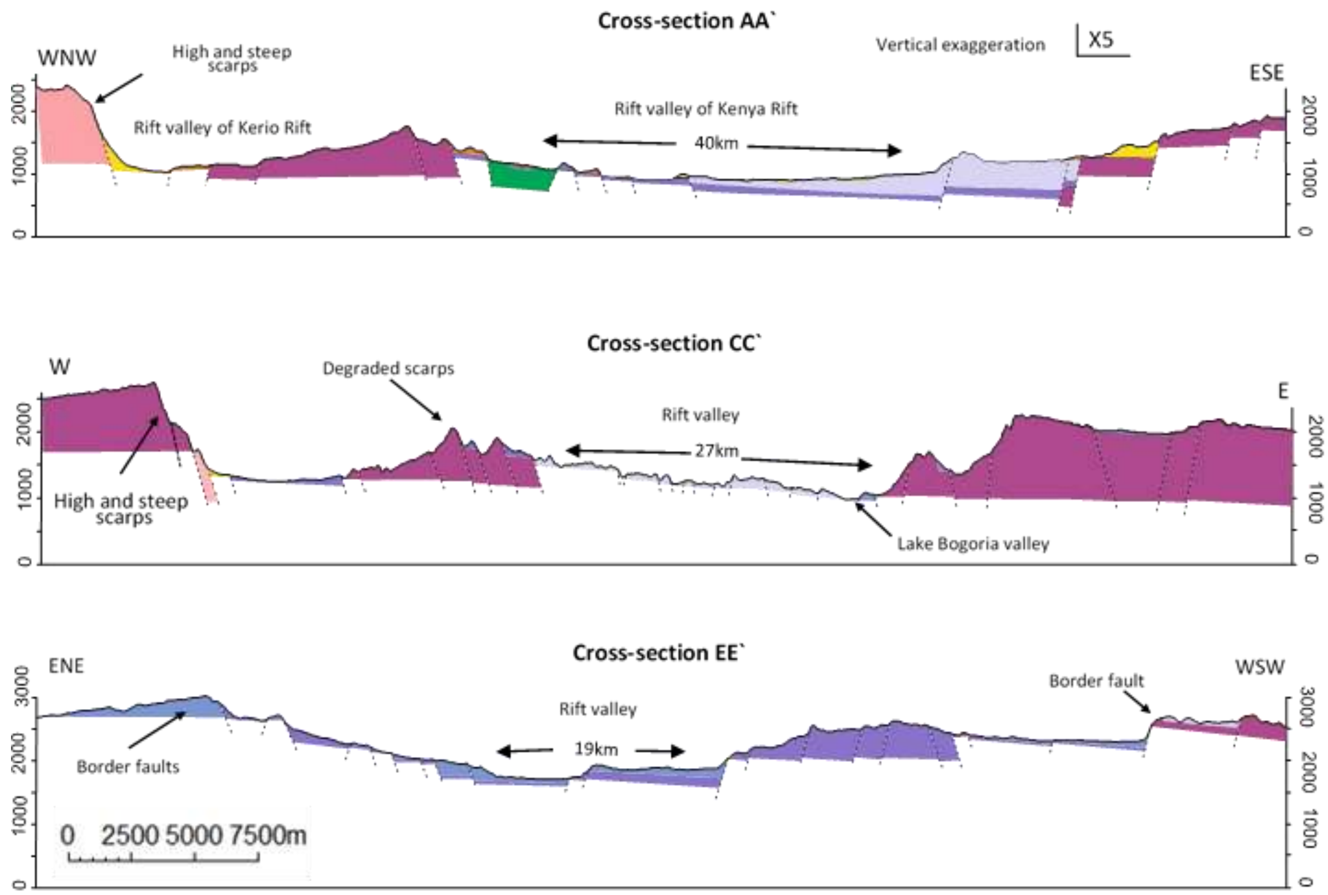

Figure 8. Cross-sections AA`, BB` & CC` displaying the topographic profile, see Figure 1 Figure 7 for locations of these cross-section and the key of the geological units.

Table 1 Total fault heaves obtained from each cross-section (Figure 7)

Zones	Zone1		Zone2		Zone3	
Cross-sections	AA`	BB`	CC`	DD`	EE`	FF `
Total heaves measurement (m), (± uncertainty)	10748 (±126)	8884 (±199)	8882 (±133)	6066 (±45)	5896 (±63)	5226 (±77)
Average of total heave (m)	9816		7474		5561	
Heave percentage %	24	19	19	13	13	11
Length of cross-sections (Km)	107	92	78	44	83	70

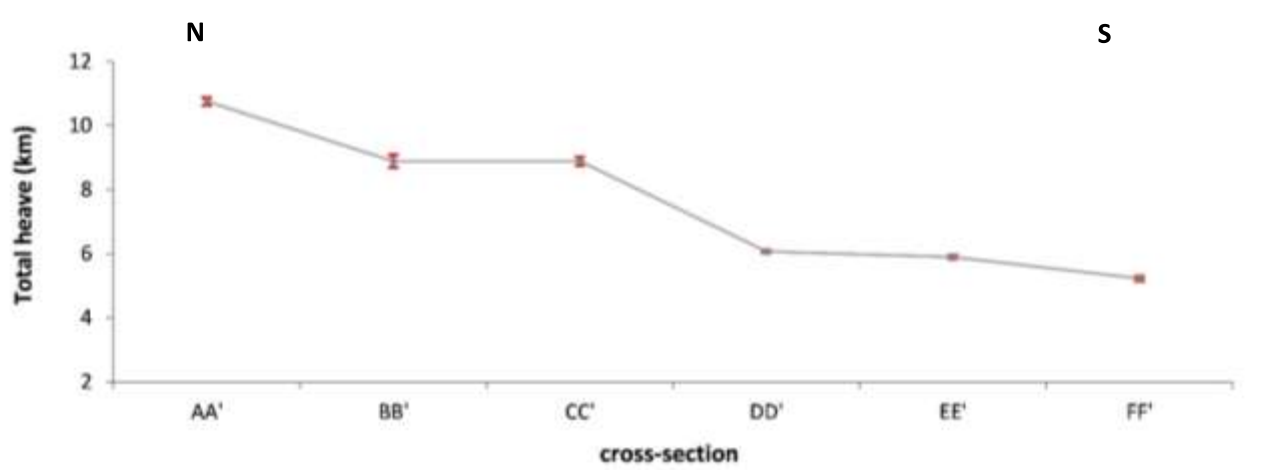

Figure 9. Illustration showing the progressive increase of total heave (which is illustrative of strain, see section 4.3) from south to north. See Figure 7 for locations of cross-sections. Red bars represent calculated error in heave measurements.

4.4 Fault displacement populations

Table 2. Results of functions fit to displacement data

Rift zone	R^2 for Function fits		
	Power-law	Log-normal	Exponential
zone 1	0.96	0.90	0.81
zone 2	0.93	0.91	0.82
zone 3	0.90	0.92	0.85
All zones	0.92	0.90	0.83

Fault displacement data for the three zones combined (Figure 10) and individually (Figure 11) were analysed using fault cumulative frequency log-log plots, and three statistical models including power law, log-normal and exponential laws were used to assess the best fit for the fault displacement populations. Generally power law scaling was found to be the best statistical model to fit the displacement data based upon the values of coefficient of determination R^2 (Table 2).

It has been shown in the literature that power law is preferred over other statistical distributions because it provides a better description of fault size distributions (e.g. Bonnet et al., 2001). For this reason, the power-law distribution is used in this study to assess the amount of deformation and to highlight the contribution of different fault sizes to the strain accommodation.

The exponents of the power-law distributions of fault displacement data from zone 1, zone 2 and zone 3 were found to be 1.0, 1.1 &1.4 respectively (Figure 11), and 1.2 for the three zones combined (Figure 10). These exponents are comparable to those obtained from a number of studies on tectonic fault systems that range from 1.0 to 1.5 (e.g. Scholz and Cowie, 1990, Marrett and Allmendinger, 1992, Gauthier and Lake, 1993, Watterson et al., 1996, Yielding et al., 1996).

It is worth mentioning that large faults do not really follow the same trend as the mid-size faults (Figure 10 & Figure 11), which might be because large faults accommodate disproportionately higher strain, leading to the steepening of population curves, as suggested by Bailey et al. (2005). Moreover, it can also be observed that there is an inverse correlation, where the lowest fractal dimension of D = 1.0 in zone 1 (Figure 10) corresponds to the largest average fault length and fault displacement of 7155 m and 660 m respectively (Table 3). On the other hand, the smallest average length and fault displacement of 5610 m and 450 m respectively corresponds to the highest fractal dimension of D = ~1.4 in zone 3; this issue is returned to later.

Table 3. Statistics of fault lengths and fault displacements in the three zones

	Length (m)			Displacement (m)		
	Min	Max	Average	Min	Max	Average
Zone 1 (n = 149)	1740	60600	7155	100	5160	660
Zone 2 (n = 295)	1270	54515	5775	40	6030	550
Zone 3 (n = 177)	1630	51477	5610	54	3939	450

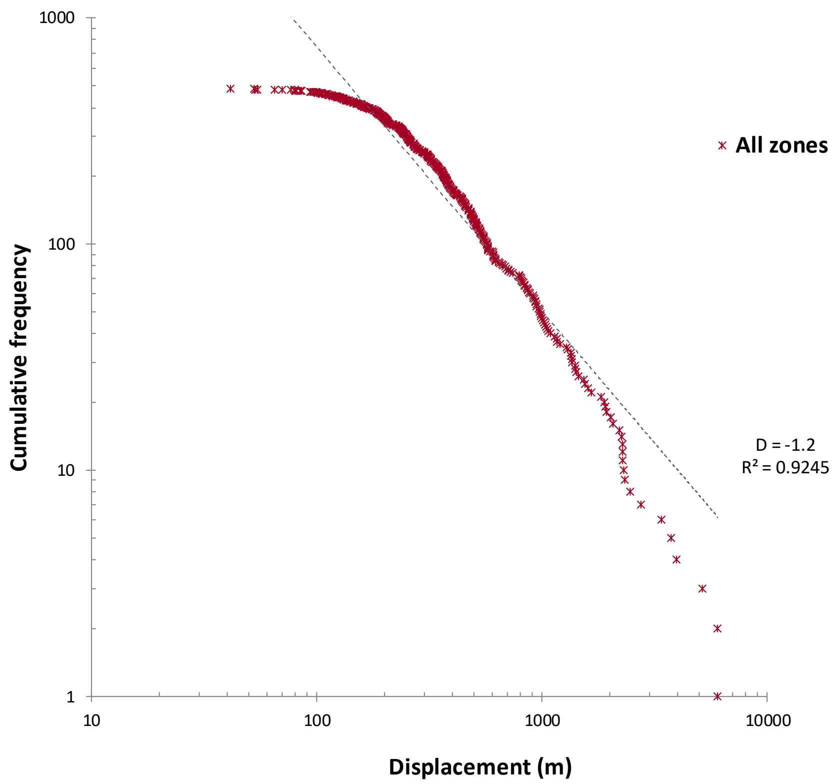

Figure 10. Displacement population showing a straight-line of power-law fitting with a slope of D = -1.2 in Log-Log plot for fault displacement against cumulative frequency for the three zones combined.

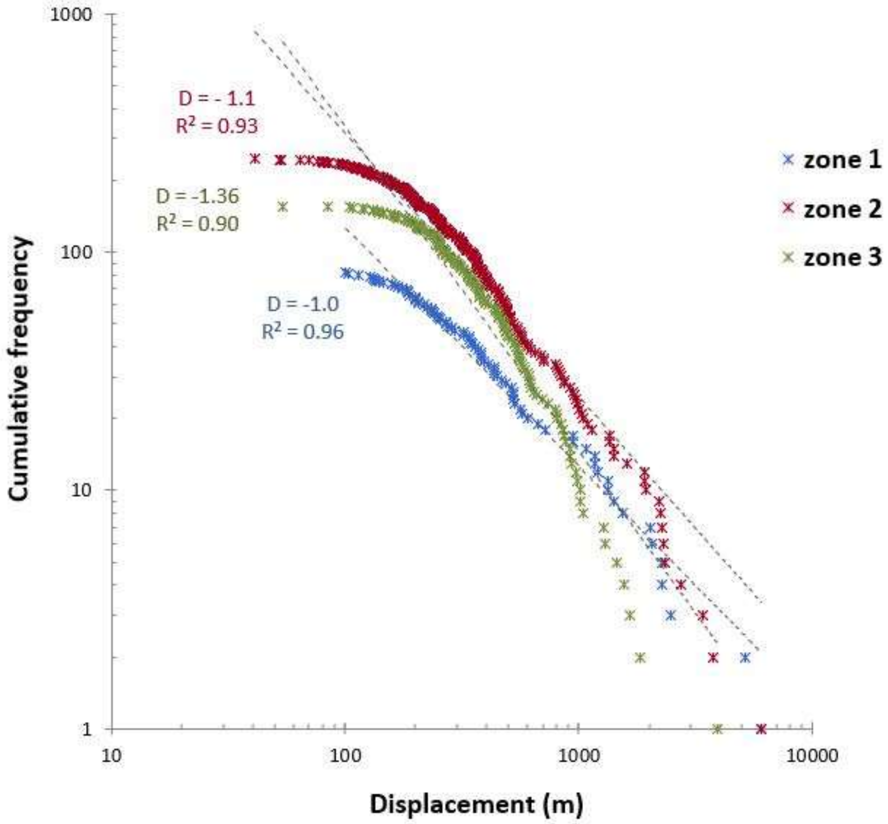

Figure 11. Log-Log plot for fault displacement against cumulative frequency for the three zones showing power-law function fit.

4.5 Fault length populations

Several studies have suggested that there is a strong correlation between fault displacement and fault length (e.g. Walsh and Watterson, 1988, Peacock and Sanderson, 1991, Cowie and Scholz, 1992a, Gillespie et al., 1993, Cartwright et al., 1995, Cowie, 1998b, Kim and Sanderson, 2005). Moreover, distribution of fault lengths should follow similar scaling relationships to fault displacement (Cladouhos and Marrett, 1996). Therefore, analysing attributes of fault length populations for the three zones using cumulative frequency function log-log plots would be expected to also show a power-law distribution. The power law exponent (D) for the length population for the three zones combined (Figure 12), and for each individual zone (Figure 13) was found to be ~1.4, which is in agreement with the range of 1.0 to 1.7 from previously published fault length populations observed in natural fault systems (e.g. Gauthier and Lake, 1993, Scholz et al., 1993, Watterson et al., 1996). We notice here that the D values for the fault traces remain almost unchanged in the three zones; the implications of this will be discussed in the next section.

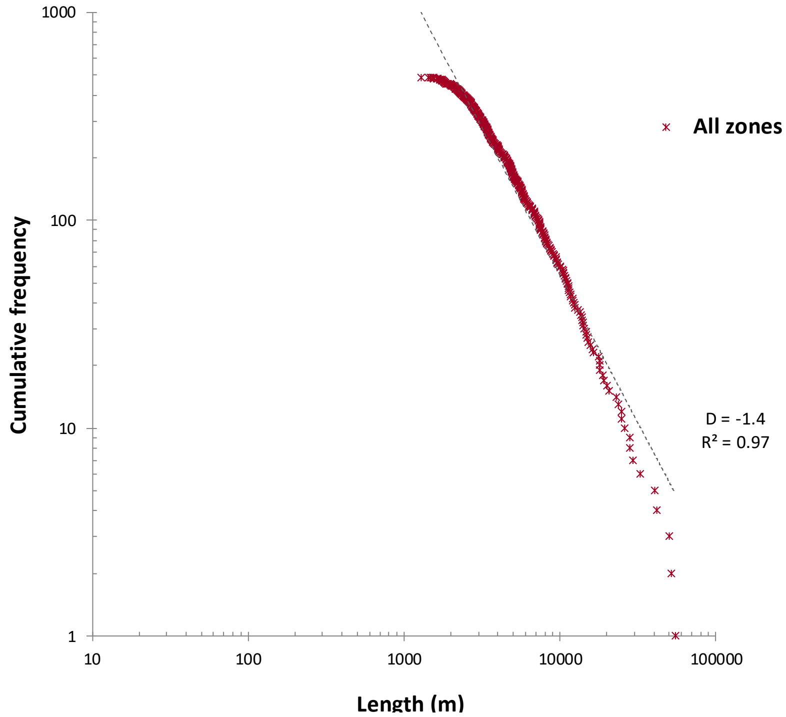

Figure 12. Log-Log plot of fault trace length vs cumulative frequency for all faults in the three zones.

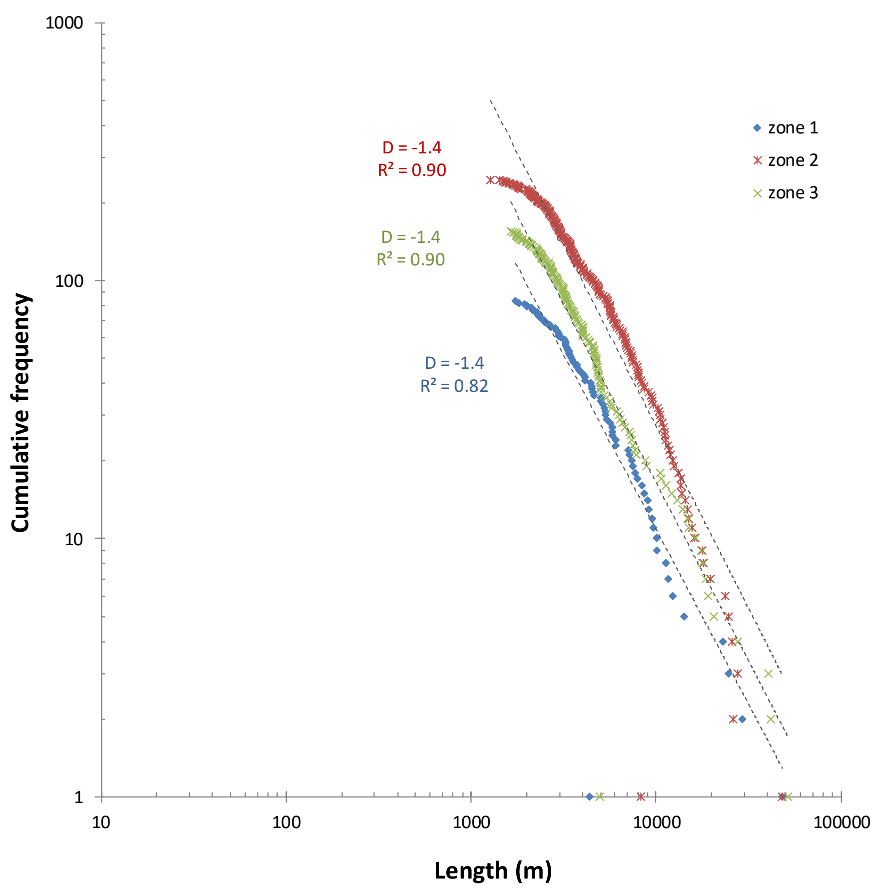

Figure 13. Log-Log plot of fault trace length vs cumulative frequency for the three zones showing power law fit.

5 Discussion

5.1 Displacement-length scatter

The datasets of 620 faults presented here is large enough to make reliable assessments and observations of changes in geometry and behaviour of fault size attributes. which may shed light on the underlying physical mechanism of fault growth and rift evolution. One possible limitation with the mapped faults in this study is that the measured fault scarp height/ throw was not fully constrained. Accumulation of sedimentary and volcanic deposits lower the apparent scarp height and would lead to underestimation of the displacement values and, in turn, extension estimates and the D\L ratios. However, this has been overcome by the application of a correction for the "hidden" throw. The displacement-length data for the mapped faults plot generally within the field of displacement-length values compiled by Gillespie et al. (1992) and Bailey et al. (2005) as shown in Figure 5. Therefore, we consider discussing results of this study in the light of published literature of normal faults to be valid.

It has been observed from displacement-length data of each individual zone (Figure 6b, c, d) that several faults have a comparable length but varying displacement. Such a vertical trend of increasing displacement for given fault length will result in an increase of displacement-length ratio for larger faults (Walsh et al., 2002a). Dawers et al. (1993) argued that the displacement-length relationship becomes non-linear in an upward increasing manner when length is considered fixed relative to the cumulative slip from many slip events. Therefore, the observed upward trend of increasing displacement population in each zone of the study area (Figure 6 b, c, d) could be explained as follows: smaller faults that have experienced fewer slip events should have lower displacement-length ratios than larger faults that have experienced more slip events. This interpretation may be valid for the mapped faults in this study that occur in a single geological setting, whilst recognising that previous research by Cowie and Scholz (1992a) suggests that the fault displacement-length ratio may also be modified by material properties of the rock or if data are combined from diverse geologic settings.

It has been mentioned in section 4 above that the scatter in any the maximum displacement-length data could be caused by several sources; errors associated with the fault picks from the DEM surface could contribute to the large scatter observed in this dataset (Figure 6). It also has been noted from the geological map of Kenya (Figure 1) that the study area is covered by Quaternary and Tertiary volcanic sediments that could be relatively uniform in lithology. Moreover, Smith (1994) indicated in his study that therefore, the lower Miocene sediments deposited in central Kenya are predominantly volcanogenic. Therefore, it could be argued that scattering shown by this dataset may be caused by other sources other than the rock lithology. Another likely source that introduces scatter to plots of maximum displacement versus length of this dataset is the process of fault growth through segment linkage, which is discussed further below.

5.2 Strain distribution

Extension regime in the central Kenya Rift is believed to occur in an approximately E-W direction, as supported by geological data (Daly et al., 1989, Morley, 1988), current seismicity (Fairhead and Stuart, 1982, Foster and Jackson, 1998) and GPS analysis (Calais et al., 2006). The central Kenya Rift is thought to be developed on a strongly heterogeneous basement, exhibiting a series of late Proterozoic, regional scale NW-SE and NS trending ductile/brittle shear zones, which exist in the lithosphere beneath the rift (Daly et al., 1989, Maurin and Guiraud, 1993, Mosley, 1993). Moreover, underlying basement fabric structures may occur such as faults (Giba et al., 2012, Bellahsen and Daniel, 2005), shear zones (Corti, 2008, Agostini et al., 2011, Corti, 2012) or foliations (Hetzel and Strecker, 1994) which could interfere with the regional stress leading to localized variations in stress orientations (Aleksandrowski et al., 1992, Teyssier and Tikoff, 1999), and influence the orientation of normal faults during their initiation and evolution (Giba et al., 2012, Bellahsen and Daniel, 2005, Agostini et al., 2009). Consequently, different orientations of fault populations observed in the three zones (zone 1, 2 &3) in the central Kenya rift under the same regional extension direction could be due to existence and influence of pre-existing structures with different orientations.

Estimation of strain through heave measurements along the study area (Figure 3.10a) exhibits that cross-sections EE` and FF` in zone 3 in the south part of the rift also cross through a relatively large number of faults but still have the least average heave percentage of ~12%, and that is because faults in zone 3 are relatively smaller in size as indicated by the smallest average fault length and displacement (see Table 3). Cross-sections CC` and DD` in zone 2 pass across a relatively larger number of faults and accommodate an average heave percentage of ~16%. On the other hand, cross-sections AA` and BB in zone 1 in the north accommodate the largest average heave percentage of ~22% along this part of the Rift. Table 3 displays that zone 1 encompasses the fewest number of resolved faults (n = 149) and has the largest average of fault trace-length and fault displacement. Therefore, differences in extensional strain accommodated between the southern and northern zones of the study area are attributable to the extensional strain localization along a few faults in the northern part (zone 1). These faults are deeper, with larger throws, and therefore take up more extensional strain than those in the southern part (zone 3). These strain estimations suggest that zone 1 accommodates the largest amount of strain, followed by zone 2 then zone 3.

5.3 Fault population analysis and implications for fault growth and rift evolution

It has been demonstrated earlier that fault populations in the three defined zones (zone 1, zone 2 and zone 3), either individually or combined have exhibited a power-law distribution for both fault length and displacement data. Fitting to a power law distribution for fault length populations in the three zones is compatible with the low-strain settings of early continental Rifting (Gupta and Scholz, 2000, Vétel et al., 2005). That contrasts with a high strain setting where rifts are more evolved and, therefore, an exponential scaling function appears in the cumulative distribution for fault lengths as observed in the North Ethiopian Rift–Afar transition area by Soliva and Schultz (2008), and in the Main Ethiopian Rift by Agostini et al. (2011).

Differences in the exponent of power law scaling of fault size population distributions are used to assess the contribution of different fault sizes to total strain accommodation (Yielding et al., 1996). The higher the exponent of population slopes, D (fractal dimension), the higher the contribution of small faults to strain accommodation (Marrett and Allmendinger, 1991, Yielding et al., 1996). This has been confirmed in the current study for the examined fault displacement distributions (Figure 11), where zone 3 in the south accommodates the least strain (Figure 9 & Table 1) and has the highest fractal dimension of D = ~1.4 (Figure 11). This implies that zone 3 encompasses a larger number of small faults contributing to the strain accommodation compared to zone 2 and zone1, and that is supported by the smallest averages of fault length and fault displacement of 5610 m and 450 m respectively calculated for zone 3 (Table 3).

In the centre of the study area, the cumulative extension in zone 2 has increased to 7474m as opposed to 5561m in zone 3 (Figure 9 & Table 1). Consequently, the power law exponent of fault displacement population decreases to D = 1.1 (Figure 11). Previous studies such as Cartwright et al. (1995) and Cladouhos and Marrett (1996)) and experimental models e.g. Sornette et al. (1993) suggest that in all fault linkage models, the fractal dimension (D value) of power-law distribution decreases systematically with increasing fault strain as faults link. Thus, our observations suggest that zone 2 (where the averages of fault length and displacement are greater than that of zone 3 as shown in Table 3) is a more mature fault zone with more fault-linkage than zone 3.

Moreover, the fractal dimension for fault displacement decreases further to 1.0 in zone 1 (Figure 11) in the north where the highest strain was estimated (Figure 9 & Table 1). It has been reported in some previous studies (e.g. Cartwright et al., 1995, Cowie et al., 1995, Cladouhos and Marrett, 1996, Ackermann et al., 2001, Walsh et al., 2003b, Moriya et al., 2005) that such a decrease of fractal dimension indicates that the deformation is increasingly localised onto fewer large faults as the fault system. This has been supported in this study by the greatest statistics of fault length and fault displacement calculated for zone 1 (Table 3) where the fewest number of faults were mapped.

However, in many cases a simple power-law may not account for the full-range of the observed scaling behaviour (Davy, 1993, Soliva and Schultz, 2008, Vétel et al., 2005). Among other factors that contribute to the complexity of the fault network evolution, the boundary condition of the brittle layer may also affect how the fault system evolves (Cowie et al., 2005, Hardacre and Cowie, 2003). Kudo and Furumoto (1998) applied the fractal dimension analysis to characterize the crustal structures in three Japanese Islands, and they observed changes in fractal dimension in the three areas, which were attributed to the lateral variation of the crustal thickness in those areas. Therefore, it is worth mentioning that seismic refraction and regional reflection studies of Henry et al. (1990a) and KRISP (1991) indicate significant variations in crustal thickness between the craton and the mobile belt along the length of the Kenya Rift. Major crustal thinning occurs along the axis of the Kenya Rift where the crustal thickness varies from 35 to 40 km in the south beneath the central part of Kenya, within the vicinity of Lake Naivasha, to 18 -20 km in the north beneath Lake Turkana. Therefore, the observed changes in fractal dimension of displacement distributions for the three zones could also be due to variations in the crustal thickness of this region. However, the abovementioned results may suggest more simply that rift zone 3 in the south is in a less mature stage than rift zone 2 in the centre, and zone 2 is less developed than rift zone1 in the northern part of the study area. This phenomenon of northward increase in continental Rift evolution was also observed in the North Ethiopian Rift–Afar transition area (Soliva and Schultz, 2008) and the Main Ethiopian Rifts (Agostini et al., 2011). These inferences suggest that the processes of progressively increasing fault system maturity and strain localization onto large faults could happen even over relatively small spatial scales (as small as this study area, 240 x 150 km) within the same rift system.

In contrast to fractal dimensions of fault displacement populations (Figure 11) that decrease with increasing strain, the power law distribution of fault length populations exhibit fractal dimensions of 1.4 (Figure 13), a value which stays almost constant in the three zones despite increasing strain along the rift (Figure 9 & Table 1). Previous studies of fault linkage suggest that fractal dimension decreases systematically with increasing fault strain (e.g. Sornette et al., 1993, Cartwright et al., 1995, Cladouhos and Marrett, 1996). Such stabilization of the fractal dimension of trace-length populations was interpreted by Poulimenos (2000) to imply that linkage cessation is an important process for the evolution of the fault population over the observed range of strains.

The observed relationship between the fractal dimension and strain for fault scaling properties is illustrated in Figure 14, which may suggest that the fractal dimensions of fault population length is independent of strain. In other words, the trace-length distribution is independent of strain and the increasing strain has no effect on the fractal dimension of the fault length population.

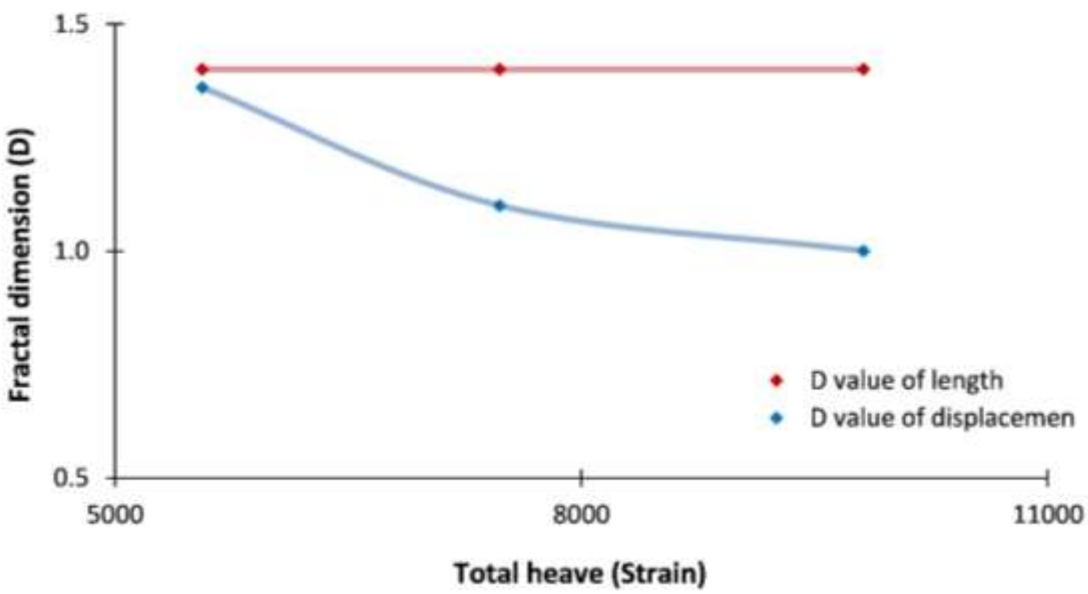

Figure 14. Illustration showing the observed relationship between the fractal dimension (D) and total heaves that represent strain for fault size attributes. Here, the D value of displacement population decreases with increasing strain, whereas the D value of length population remains almost constant as strain increases.

This would mean that with increasing strain, fault displacement increases, but fault lengths remain near constant. Moreover, these inferences support the observation of the vertical spread in the displacement population noticed in each zone of the study area (Figure 6 b, c, d). In this regard, this is consistent with the view that faults typically grow by steep or vertical growth trends rather than progressive increases both in displacement and in length (Walsh et al., 2002a, Nicol et al., 2010, Rotevatn et al., 2019). Similarly, vertical growth trends have also been observed in a natural normal fault system in the Timor Sea (Walsh et al., 2002a) and in analogue modelling (Schlagenhauf et al., 2008). Vertical growth trends like these require that, after initial rapid propagation, faults do not grow significantly in length (Walsh et al., 2002a, Nicol et al., 2010, Rotevatn et al., 2019). Therefore, these inferences are in line with the alternative/ coherent/ constant-length fault growth model suggested in previous studies (Walsh et al., 2002a, Walsh et al., 2003a, Childs et al., 2009, Giba et al., 2012, Jackson and Rotevatn, 2013, Rotevatn et al., 2019, Jackson et al., 2017, Nicol et al., 2016). This model has recently been referred to as the coherent constant-length model (Nicol et al., 2020). In that model, faults grow by rapidly establishing their near-maximum fault length in an early phase of deformation followed by accumulation of displacement with limited fault tip propagation. In this model, when strain fields of nearby isolated faults start to overlap and interact, as fault interactions are an essential feature of all fault systems (Walsh and Watterson, 1991), we see the instantaneous increase in fault length achieved by the coalescence and linkage of previously isolated faults (Walsh et al., 2002a, Rotevatn et al., 2019). The linked faults then begin to accrue displacement with no or little fault lengthening (Cartwright et al., 1995). This process will result in the creation of large localized faults. It has been mentioned above that the process of fault growth through segment linkage is an important factor to cause scatter in maximum displacement-length data (e.g. Cartwright et al., 1995, Mansfield and Cartwright, 2001). Therefore, segmented fault geometries could be responsible for the scatter in this dataset, which complicates the establishment of any scaling law.

The rapid growth of fault length to near-maximum in the early stages of rifting has also been observed further north in the Turkana Rift, north Kenya by Vétel et al. (2005) using fault displacement and length data derived from outcrop studies, and digital elevation models. Moreover, the fault growth model is found to be a dominant behaviour of normal fault growth in many extensional settings (e.g. Walsh et al., 2002a, Walsh et al., 2003a, Giba et al., 2012). Therefore, the coherent constant-length model appears to be the most plausible scenario for the mode of normal fault growth in the study area.

A study by Poulimenos (2000) in the active basin of the western Corinth Graben of central Greece, and another study by Meyer et al. (2002) in the Vulcan Sub-basin of the Timor Sea, northwest Australia examined fault growth of normal faults using fractal dimension analysis of fault size populations. Both studies reached a similar conclusion to the current one, where fault lengths were established early during extension of the basin and a later extension was largely accommodated by accumulation of displacements with minimal fault propagation. However, those studies could not establish the generality of their findings due to lack of detailed studies of the growth of fault populations with which their conclusions can be compared. Thus, having compared the current study with those studies, it can be concluded that, in active extensional setting, fractal dimension analysis appears to be a useful factor to describe the displacement-length relationship in case the high scatter in displacement-length does not help in understanding the growth of normal faults.

6 Conclusion

620 normal faults have been mapped from ASTER DEM surface data within the central Kenya Rift. Fault trace lengths were corrected for resolution bias, and the extent of total fault throw into the subsurface was estimated. The maximum displacement was therefore calculated using an average dip value for the study area. Three fault populations have been identified within the study area according to their average fault strike as zone 1 in the north, zone 2 in the centre & zone 3 in the south. The wide scale range of fault size populations (maximum displacement of ~40 – ~6030 m; lengths of 1270 m to 60600 m) contained within the data, allowed quantitative assessment of the scaling properties of the three fault populations, in order to inform our understanding of the growth of normal faults. Estimations of extensional strain obtained from six transects along the rift revealed a general increase of strain northward. Fault displacement data, analysed by the cumulative frequency, obey a power-law distribution for the three zones of fault populations with fractal dimension D of 1.0, 1.1 &1.4 for zone 1, zone 2 and zone 3 respectively. Fault trace-length data also conform to the same power-law relationships, but with D Values of ~1.4 for all three zones. Values of fractal dimension of displacement distribution for the three zones showed a decrease with increasing strain as we move from the south (zone3) through the centre (zone2) to the north (zone1) along the rift, which implies that the strain is increasingly localised onto larger faults as the fault system evolves. In addition, values of fractal dimension of fault length distributions remained almost unchanged in the three zones even with increasing strain. Increasing fault displacement whilst the length remains almost fixed with increasing strain along the study area may suggest that the fault system could be evolving in accordance to the coherent constant-length fault growth model. Therefore, findings of this study suggest that the evolution of rift deformation, can be observed even over relatively short spatial scales. It has also been concluded that patterns of fault growth can be deduced from fractal dimension of cumulative distribution of fault size populations.

7 References

ACKERMANN, R. V. & SCHLISCHE, R. W. 1997. Anticlustering of small normal faults around larger faults. *Geology,* 25, 1127-1130.

ACKERMANN, R. V., SCHLISCHE, R. W. & WITHJACK, M. O. 2001. The geometric and statistical evolution of normal fault systems: an experimental study of the effects of mechanical layer thickness on scaling laws. *Journal of Structural Geology,* 23, 1803-1819.

AGOSTINI, A., BONINI, M., CORTI, G., SANI, F. & MAZZARINI, F. 2011. Fault architecture in the Main Ethiopian Rift and comparison with experimental models: Implications for rift evolution and Nubia–Somalia kinematics. *Earth and Planetary Science Letters,* 301, 479-492.

AGOSTINI, A., BONINI, M., CORTI, G., SANI, F. & MAZZARINI, F. 2011b. Fault architecture in the Main Ethiopian Rift and comparison with experimental models: Implications for rift evolution and Nubia–Somalia kinematics. *Earth and Planetary Science Letters,* 301, 479-492.

AGOSTINI, A., CORTI, G., ZEOLI, A. & MULUGETA, G. 2009. Evolution, pattern, and partitioning of deformation during oblique continental rifting: Inferences from lithospheric-scale centrifuge models. *Geochemistry, Geophysics, Geosystems,* 10, Q11015.

ALEKSANDROWSKI, P., INDERHAUG, O. H. & KNAPSTAD, B. 1992. Tectonic structures and wellbore breakout orientation. *The 33th U.S. Symposium on Rock Mechanics (USRMS).* Santa Fe, New Mexico: American Rock Mechanics Association.

BAILEY, W. R., WALSH, J. J. & MANZOCCHI, T. 2005. Fault populations, strain distribution and basement fault reactivation in the East Pennines Coalfield, UK. *Journal of Structural Geology,* 27, 913-928.

BAKER, B. H., MITCHELL, J. G. & WILLIAMS, L. A. J. 1988. Stratigraphy, geochronology and volcano-tectonic evolution of the Kedong–Naivasha–Kinangop region, Gregory Rift Valley, Kenya. *Journal of the Geological Society,* 145, 107-116.

BAKER, B. H., MOHR, P. A. & WILLIAMS, L. A. J. 1972. Geology of the Eastern Rift System of Africa. *Geological Society of America Special Papers,* 136, 1-68.

BAKER, B. H. & WOHLENBERG, J. 1971. Structure and Evolution of the Kenya Rift Valley. *Nature,* 229, 538-542.

BELLAHSEN, N. & DANIEL, J. M. 2005. Fault reactivation control on normal fault growth: an experimental study. *Journal of Structural Geology,* 27, 769-780.

BONNET, E., BOUR, O., ODLING, N. E., DAVY, P., MAIN, I., COWIE, P. & BERKOWITZ, B. 2001. Scaling of fracture systems in geological media. *Reviews of Geophysics,* 39, 347-383.

CALAIS, E., EBINGER, C., HARTNADY, C. & NOCQUET, J. M. 2006. Kinematics of the East African Rift from GPS and earthquake slip vector data. *Geological Society, London, Special Publications,* 259, 9-22.

CARTWRIGHT, J. A., MANSFIELD, C. & TRUDGILL, B. 1996. The growth of normal faults by segment linkage. *Geological Society, London, Special Publications,* 99, 163-177.

CARTWRIGHT, J. A., TRUDGILL, B. D. & MANSFIELD, C. S. 1995. Fault growth by segment linkage: an explanation for scatter in maximum displacement and trace length data from the Canyonlands Grabens of SE Utah. *Journal of Structural Geology,* 17, 1319-1326.

CHILDS, C., MANZOCCHI, T., WALSH, J. J., BONSON, C. G., NICOL, A. & SCHÖPFER, M. P. J. 2009. A geometric model of fault zone and fault rock thickness variations. *Journal of Structural Geology,* 31, 117-127.

CHOROWICZ, J. 2005. The East African rift system. *Journal of African Earth Sciences,* 43, 379-410.

CLADOUHOS, T. T. & MARRETT, R. 1996. Are fault growth and linkage models consistent with power-law distributions of fault lengths? *Journal of Structural Geology,* 18, 281-293.

CORTI, G. 2008. Control of rift obliquity on the evolution and segmentation of the main Ethiopian rift. *Nature Geoscience,* 1, 258-262.

CORTI, G. 2009. Continental rift evolution: From rift initiation to incipient break-up in the Main Ethiopian Rift, East Africa. *Earth-Science Reviews,* 96, 1-53.

CORTI, G. 2012. Evolution and characteristics of continental rifting: Analog modeling-inspired view and comparison with examples from the East African Rift System. Volumes 522–523, Pages 1–33.

COWIE, P. A. 1998a. Normal fault growth in three dimensions in continental and oceanic crust. *GEOPHYSICAL MONOGRAPH-AMERICAN GEOPHYSICAL UNION,* 106, 325-348.

COWIE, P. A. 1998b. A healing–reloading feedback control on the growth rate of seismogenic faults. *Journal of Structural Geology,* 20, 1075-1087.

COWIE, P. A. & SCHOLZ, C. H. 1992a. Displacement-length scaling relationship for faults: data synthesis and discussion. *Journal of Structural Geology,* 14, 1149-1156.

COWIE, P. A. & SCHOLZ, C. H. 1992b. Growth of faults by accumulation of seismic slip. *Journal of Geophysical Research: Solid Earth,* 97, 11085-11095.

COWIE, P. A., SORNETTE, D. & VANNESTE, C. 1995. Multifractal scaling properties of a growing fault population. *Geophysical Journal International,* 122, 457-469.

COWIE, P. A., UNDERHILL, J. R., BEHN, M. D., LIN, J. & GILL, C. E. 2005. Spatio-temporal evolution of strain accumulation derived from multi-scale observations of Late Jurassic rifting in the northern North Sea: A critical test of models for lithospheric extension. *Earth and Planetary Science Letters,* 234, 401-419.

DALY, M. C., CHOROWICZ, J. & FAIRHEAD, J. D. 1989. Rift basin evolution in Africa: the influence of reactivated steep basement shear zones. *Geological Society, London, Special Publications,* 44, 309-334.

DAVIS, K., BURBANK, D. W., FISHER, D., WALLACE, S. & NOBES, D. 2005. Thrust-fault growth and segment linkage in the active Ostler fault zone, New Zealand. *Journal of Structural Geology,* 27, 1528-1546.

DAVY, P. 1993. On the frequency-length distribution of the San Andreas fault system. *Journal of Geophysical Research: Solid Earth,* 98, 12141-12151.

DAWERS, N. H., ANDERS, M. H. & SCHOLZ, C. H. 1993. Growth of normal faults: Displacement-length scaling. *Geology,* 21, 1107-1110.

EBINGER, C. J. 1989. Tectonic development of the western branch of the East African rift system. *Geological Society of America Bulletin,* 101, 885-903.

FAIRHEAD, J. D. & STUART, G. W. 1982. The Seismicity of the East African Rift System and Comparison with Other Continental Rifts. *Continental and Oceanic Rifts.* American Geophysical Union.

FOSSEN, H. & HESTHAMMER, J. 1997. Geometric analysis and scaling relations of deformation bands in porous sandstone. *Journal of Structural Geology,* 19, 1479-1493.

FOSTER, A. N. & JACKSON, J. A. 1998. Source parameters of large African earthquakes: implications for crustal rheology and regional kinematics. *Geophysical Journal International,* 134, 422-448.

GAUTHIER, B. & LAKE, S. 1993. Probabilistic modeling of faults below the limit of seismic resolution in Pelican Field, North Sea, offshore United Kingdom. *AAPG Bulletin,* 77, 761-777.

GIBA, M., WALSH, J. J. & NICOL, A. 2012. Segmentation and growth of an obliquely reactivated normal fault. *Journal of Structural Geology,* 39**,** 253-267.

GILLESPIE, P. A., HOWARD, C. B., WALSH, J. J. & WATTERSON, J. 1993. Measurement and characterisation of spatial distributions of fractures. *Tectonophysics,* 226**,** 113-141.

GILLESPIE, P. A., WALSH, J. J. & WATTERSON, J. 1992. Limitations of dimension and displacement data from single faults and the consequences for data analysis and interpretation. *Journal of Structural Geology,* 14**,** 1157-1172.

GILLESPIE, P. A., WALSH, J. J., WATTERSON, J., BONSON, C. G. & MANZOCCHI, T. 2001. Scaling relationships of joint and vein arrays from The Burren, Co. Clare, Ireland. *Journal of Structural Geology,* 23**,** 183-201.

GUPTA, A. & SCHOLZ, C. H. 2000. Brittle strain regime transition in the Afar depression: Implications for fault growth and seafloor spreading. *Geology,* 28**,** 1087-1090.

HARDACRE, K. M. & COWIE, P. A. 2003. Controls on strain localization in a two-dimensional elastoplastic layer: Insights into size-frequency scaling of extensional fault populations. 108.

HAUTOT, S., TARITS, P., WHALER, K., LE GALL, B., TIERCELIN, J.-J. & LE TURDU, C. 2000. Deep structure of the Baringo Rift Basin (central Kenya) from three-dimensional magnetotelluric imaging: Implications for rift evolution. *Journal of Geophysical Research: Solid Earth,* 105**,** 23493-23518.

HEFFER, K. & BEVAN, T. Scaling relationships in natural fractures: data, theory, and application. European Petroleum Conference, 1990. Society of Petroleum Engineers.

HENRY, W. J., MECHIE, J., MAGUIRE, P., KHAN, M., PRODEHL, C., KELLER, G. & PATEL, J. 1990a. A seismic investigation of the Kenya Rift Valley. *Geophysical Journal International,* 100**,** 107-130.

HENRY, W. J., MECHIE, J., MAGUIRE, P. K. H., KHAN, M. A., PRODEHL, C., KELLER, G. R. & PATEL, J. 1990b. A Seismic Investigation of the Kenya Rift Valley. *Geophysical Journal International,* 100**,** 107-130.

HETZEL, R. & STRECKER, M. R. 1994. Late Mozambique Belt structures in western Kenya and their influence on the evolution of the Cenozoic Kenya Rift. *Journal of Structural Geology,* 16**,** 189-201.

JACKSON, C. A.-L., BELL, R. E., ROTEVATN, A. & TVEDT, A. B. 2017. Techniques to determine the kinematics of synsedimentary normal faults and implications for fault growth models. *Geological Society, London, Special Publications,* 439**,** 187-217.

JACKSON, C. A.-L. & ROTEVATN, A. 2013. 3D seismic analysis of the structure and evolution of a salt-influenced normal fault zone: a test of competing fault growth models. *Journal of Structural Geology,* 54**,** 215-234.

JACKSON, P. & SANDERSON, D. J. 1992. Scaling of fault displacements from the Badajoz-Cordoba shear zone, SW Spain. *Tectonophysics,* 210**,** 179-190.

JONES, W. B. & LIPPARD, S. J. 1979. New age determinations and the geology of the Kenya Rift-Kavirondo Rift junction, W Kenya. *Journal of the Geological Society,* 136**,** 693-704.

KIM, Y.-S. & SANDERSON, D. J. 2005. The relationship between displacement and length of faults: a review. *Earth-Science Reviews,* 68**,** 317-334.

KRISP, W. G. 1991. Large-scale variation in lithospheric structure along and across the Kenya rift *Nature,* 354.

KUDO, T. & FURUMOTO, M. 1998. Characterization of crustal structures by fractal analysis of gravity anomalies. *Proceedings of the Japan Academy, Series B,* 74**,** 69-74.

LE GALL, B., NONNOTTE, P., ROLET, J., BENOIT, M., GUILLOU, H., MOUSSEAU-NONNOTTE, M., ALBARIC, J. & DEVERCHÈRE, J. 2008. Rift propagation at craton margin.: Distribution of faulting and volcanism in the North Tanzanian Divergence (East Africa) during Neogene times. *Tectonophysics,* 448**,** 1-19.

MANSFIELD, C. & CARTWRIGHT, J. 2001. Fault growth by linkage: observations and implications from analogue models. *Journal of Structural Geology,* 23**,** 745-763.

MARIITA, N. O. & KELLER, G. R. 2007. An integrated geophysical study of the northern Kenya rift. *Journal of African Earth Sciences,* 48**,** 80-94.

MARRETT, R. & ALLMENDINGER, R. W. 1991. Estimates of strain due to brittle faulting: sampling of fault populations. *Journal of Structural Geology,* 13**,** 735-738.

MARRETT, R. & ALLMENDINGER, R. W. 1992. Amount of extension on "small" faults: An example from the Viking graben. *Geology,* 20**,** 47-50.

MAURIN, J.-C. & GUIRAUD, R. 1993. Basement control in the development of the early cretaceous West and Central African rift system. *Tectonophysics,* 228**,** 81-95.

MCCONNELL, R. B. 1972. Geological Development of the Rift System of Eastern Africa. *Geological Society of America Bulletin,* 83**,** 2549-2572.

MEYER, V., NICOL, A., CHILDS, C., WALSH, J. & WATTERSON, J. 2002. Progressive localisation of strain during the evolution of a normal fault population. *Journal of Structural Geology,* 24**,** 1215-1231.

MORIYA, S., CHILDS, C., MANZOCCHI, T. & WALSH, J. J. 2005. Analysis of the relationships between strain, polarity and population slope for normal fault systems. *Journal of Structural Geology,* 27**,** 1113-1127.

MORLEY, C. 1988. Variable extension in lake Tanganyika. *Tectonics,* 7**,** 785-801.

MORLEY, C. & NGENOH, D. 1999c. AAPG Studies in Geology# 44, Chapter 1: Introduction to the East African Rift System.

MOSLEY, P. N. 1993. Geological evolution of the late Proterozoic “Mozambique Belt” of Kenya. *Tectonophysics,* 221**,** 223-250.

NGENOH, D. K. A. 1993. Hydrocarbon potential of South Kerio Trough basin (Kenya) from seismic reflection data. *M.Sc. thesis, University of Western Ontario: London, Canada 126 pp.*

NICOL, A., CHILDS, C., WALSH, J. J., MANZOCCHI, T. & SCHÖPFER, M. P. J. 2016. Interactions and growth of faults in an outcrop-scale system. *Geological Society, London, Special Publications,* 439.

NICOL, A., WALSH, J., CHILDS, C. & MANZOCCHI, T. 2020. The growth of faults. *Understanding Faults.* Elsevier.

NICOL, A., WALSH, J., VILLAMOR, P., SEEBECK, H. & BERRYMAN, K. 2010. Normal fault interactions, paleoearthquakes and growth in an active rift. *Journal of Structural Geology,* 32**,** 1101-1113.

OMENDA, P. A. 2010. THE GEOLOGY AND GEOTHERMAL ACTIVITY OF THE EAST AFRICAN RIFT.

PEACOCK, D. 2002. Propagation, interaction and linkage in normal fault systems. *Earth-Science Reviews,* 58**,** 121-142.

PEACOCK, D. C. P. & SANDERSON, D. J. 1991. Displacements, segment linkage and relay ramps in normal fault zones. *Journal of Structural Geology,* 13**,** 721-733.

PETIT, C. & EBINGER, C. 2000. Flexure and mechanical behavior of cratonic lithosphere: Gravity models of the East African and Baikal rifts. *Journal of Geophysical Research: Solid Earth,* 105**,** 19151-19162.

PICKERING, G., BULL, J. M. & SANDERSON, D. J. 1995. Sampling power-law distributions. *Tectonophysics,* 248**,** 1-20.

PICKERING, G., PEACOCK, D. C. P. & LEE, J. M. 1997. Modeling Tip Zones to Predict the Throw and Length Characteristics of Faults1. *AAPG Bulletin,* 81**,** 82-99.

POPE, D. A. 1992. Analyses and interpretations of the seismic reflection profiles from the Kerio Valley, Kenya Rift. *M.Sc. thesis, University of Leeds (1992), p. 133*.

POULIMENOS, G. 2000. Scaling properties of normal fault populations in the western Corinth Graben, Greece: implications for fault growth in large strain settings. *Journal of Structural Geology,* 22**,** 307-322.

ROTEVATN, A., JACKSON, C. A. L., TVEDT, A. B. M., BELL, R. E. & BLÆKKAN, I. 2019. How do normal faults grow? *Journal of Structural Geology,* 125**,** 174-184.

SCHLAGENHAUF, A., MANIGHETTI, I., MALAVIEILLE, J. & DOMINGUEZ, S. 2008. Incremental growth of normal faults: Insights from a laser-equipped analog experiment. *Earth and Planetary Science Letters,* 273**,** 299-311.

SCHLISCHE, R. W., YOUNG, S. S., ACKERMANN, R. V. & GUPTA, A. 1996. Geometry and scaling relations of a population of very small rift-related normal faults. *Geology,* 24**,** 683-686.

SCHOLZ, C. H. & COWIE, P. A. 1990. Determination of total strain from faulting using slip measurements. *Nature,* 346**,** 837-839.

SCHOLZ, C. H., DAWERS, N. H., YU, J. Z., ANDERS, M. H. & COWIE, P. A. 1993. Fault growth and fault scaling laws: Preliminary results. *Journal of Geophysical Research: Solid Earth,* 98**,** 21951-21961.

SCHULTZ, R. A. & FOSSEN, H. 2002. Displacement–length scaling in three dimensions: the importance of aspect ratio and application to deformation bands. *Journal of Structural Geology,* 24**,** 1389-1411.

SMITH, M. 1994. Stratigraphic and structural constraints on mechanisms of active rifting in the Gregory Rift, Kenya. *Tectonophysics,* 236**,** 3-22.

SMITH, M. & MOSLEY, P. 1993. Crustal heterogeneity and basement influence on the development of the Kenya Rift, East Africa. *Tectonics,* 12**,** 591-606.

SOLIVA, R., BENEDICTO, A. & MAERTEN, L. 2006. Spacing and linkage of confined normal faults: Importance of mechanical thickness. *Journal of Geophysical Research: Solid Earth,* 111**,** n/a-n/a.

SOLIVA, R. & SCHULTZ, R. A. 2008. Distributed and localized faulting in extensional settings: Insight from the North Ethiopian Rift–Afar transition area. *Tectonics,* 27**,** n/a-n/a.

SORNETTE, A., DAVY, P. & SORNETTE, D. 1993. Fault growth in brittle-ductile experiments and the mechanics of continental collisions. *Journal of Geophysical Research: Solid Earth,* 98**,** 12111-12139.

STANTON-YONGE, A., CEMBRANO, J., GRIFFITH, W., JENSEN, E. & MITCHELL, T. 2020. Self-similar length-displacement scaling achieved by scale-dependent growth processes: Evidence from the Atacama Fault System. *Journal of Structural Geology,* 133**,** 103993.

TEYSSIER, C. & TIKOFF, B. 1999. Fabric stability in oblique convergence and divergence. *Journal of Structural Geology,* 21**,** 969-974.

TORABI, A., ALAEI, B. & LIBAK, A. 2019. Normal fault 3D geometry and displacement revisited: Insights from faults in the Norwegian Barents Sea. *Marine and Petroleum Geology,* 99**,** 135-155.

TORABI, A. & BERG, S. S. 2011. Scaling of fault attributes: A review. *Marine and Petroleum Geology,* 28**,** 1444-1460.

VÉTEL, W., LE GALL, B. & WALSH, J. J. 2005. Geometry and growth of an inner rift fault pattern: the Kino Sogo Fault Belt, Turkana Rift (North Kenya). *Journal of Structural Geology,* 27, 2204-2222.

WALSH, J., NICOL, A. & CHILDS, C. A New Model for the Growth of Faults. 64th EAGE Conference & Exhibition, 2002b.

WALSH, J., WATTERSON, J. & YIELDING, G. 1991. The importance of small-scale faulting in regional extension. *Nature,* 351, 391-393.

WALSH, J. J., BAILEY, W. R., CHILDS, C., NICOL, A. & BONSON, C. G. 2003a. Formation of segmented normal faults: a 3-D perspective. *Journal of Structural Geology,* 25, 1251-1262.

WALSH, J. J., CHILDS, C., IMBER, J., MANZOCCHI, T., WATTERSON, J. & NELL, P. A. R. 2003b. Strain localisation and population changes during fault system growth within the Inner Moray Firth, Northern North Sea. *Journal of Structural Geology,* 25, 307-315.

WALSH, J. J., NICOL, A. & CHILDS, C. 2002a. An alternative model for the growth of faults. *Journal of Structural Geology,* 24, 1669-1675.

WALSH, J. J. & WATTERSON, J. 1988. Analysis of the relationship between displacements and dimensions of faults. *Journal of Structural Geology,* 10, 239-247.

WALSH, J. J. & WATTERSON, J. 1991. Geometric and kinematic coherence and scale effects in normal fault systems. *Geological Society, London, Special Publications,* 56, 193-203.

WALSH, J. J., WATTERSON, J., CHILDS, C. & NICOL, A. 1996. Ductile strain effects in the analysis of seismic interpretations of normal fault systems. *Geological Society, London, Special Publications,* 99, 27-40.

WATTERSON, J. 1986. Fault dimensions, displacements and growth. *pure and applied geophysics,* 124, 365-373.

WATTERSON, J., WALSH, J. J., GILLESPIE, P. A. & EASTON, S. 1996. Scaling systematics of fault sizes on a large-scale range fault map. *Journal of Structural Geology,* 18, 199-214.

YIELDING, G., NEEDHAM, T. & JONES, H. 1996. Sampling of fault populations using sub-surface data: a review. *Journal of Structural Geology,* 18, 135-146.

ZHANG, L. & EINSTEIN, H. H. 2000. Estimating the intensity of rock discontinuities. *International Journal of Rock Mechanics and Mining Sciences,* 37, 819-837.

ZIEGLER, P. A. & CLOETINGH, S. 2004. Dynamic processes controlling evolution of rifted basins. *Earth-Science Reviews,* 64, 1-50.

ZIELKE, O. & STRECKER, M. R. 2009. Recurrence of Large Earthquakes in Magmatic Continental Rifts: Insights from a Paleoseismic Study along the Laikipia–Marmanet Fault, Subukia Valley, Kenya Rift. *Bulletin of the Seismological Society of America,* 99, 61-70.